Optimal Control of Non-Isothermal Viscoelastic Fluid Flow

K. Kunisch*, X. Marduel*
Karl Franzens Universität A-8010 Graz, Austria
karl.kunisch@kfunigraz.ac.at
xavier.marduel@kfunigraz.ac.at

April 16, 1999

Abstract

Optimal control of viscoelastic fluid flow in a 4 to 1 contracting channel is investigated. The control mechanism is based on heating or cooling the fluid along a portion of the boundary of the flow domain. In order to perform the control, a non-isothermal model for viscoelastic fluids is used consisting of the PTT model with relaxation time and elastic viscosity depending on temperature (following an exponential dependency, the WLF model). Moreover, the momentum, mass and constitutive equations are coupled with the heat equation forming the so-called primal system. The goal of the control is to find an optimal temperature on the boundary of the domain such that the large recirculation zones at the corners of the contracting channel are reduced and the fluid behaves like a viscous one. Two different cost functionals are used to reach this goal : one of tracking type, the other penalizing negative contributions of the velocity component in direction of the span of the channel. The minimization of these cost functionals is achieved with a gradient algorithm. An optimality system, derived by the use of the Lagrange multipliers, allows us to deduce this optimal control. The primal and dual systems are solved using the same numerical method : a finite differences discretisation on staggered grids, a decoupling approach and the Gauss-Seidel solver with a multigrid algorithm. Numerical simulations are performed with a Weissenberg number equal to 10. We succeed in reducing the recirculation zone by applying the correct boundary temperature.

Keywords : Optimal Control, Adjoint System, Finite Differences, Multigrid Algorithm, PTT Model, Non-Isothermal Flows, Viscoelastic Flow.

1 Introduction

In recent years there is an increased interest in the optimal control of fluids both from the theoretical and the numerical points of view. An optimal control problem typically consists in determining the control variables which can be external forces acting on the physical boundaries of the domain in such a manner that a pre-specified cost criterion is optimized. The problem must be solved "automatically" by means of optimization principles rather than by obtaining some suboptimal solution based on comparing the effects of different choices of the control variables on the flow field.

*SFB - Optimierung und Kontrolle

For optimal control of incompressible viscous flow significant research has been made over the last years. We can only mention some of the contributions here by referring to [Gunzburger [10][11], Glowinski [9], Temam [1], Choi [5], Ito [13], Kunisch [16], Ravindran [14], Fursikov [7], Gad-el-Hak [8]] and the references given there. The control of viscoelastic flow, only the other hand has received little, if any, attention.

The present research is intended to make a first contribution to the theory of optimal control of viscoelastic fluids. As a model problem we choose the control of the recirculation regions of a viscoelastic fluid in the corners of a suddenly contracting channel, see Fig 2. The control variables are the temperature along a portion of the boundary of the channel. More precisely, we fix a model for non-isothermal flow of a viscoelastic fluid which contains a governing equation for the temperature distribution. The boundary conditions for this thermal equation contain forcing functions corresponding to heating and cooling of the fluid. These are the (functional) control variables of our control system. The cost-functional to be minimized by the heating/cooling regime are chosen such that the recirculation zone as well as the energy of the fluid in this zone become small. The choice of a successful functional to achieve this goal is not at all a-priori clear. One of the functionals that we successfully employed is of tracking type, with the viscoelastic flow being tracked to the flow corresponding to the viscous flow modelled by the Navier Stokes equations, for which it is known that the recirculation region is significantly smaller.

Let us briefly point at some of the difficulties that need to be overcome solve our project. At first it appears to be not at all obvious, whether the influence of thermal boundary controls is sufficiently strong to successfully influence the recirculation zone. As for the heating/cooling regime it is difficult to anticipate good initial guesses. Thus the numerical optimization algorithm must be sufficiently global to converge with poor initial guesses. Finally, the viscoelastic model itself present a numerical challenge. Here it is coupled with the thermal equation and, as we shall see in Section 3, the solution of the optimal control problem requires us to solve nonlinear systems that are approximately twice as large a the system modelling the non-isothermal viscoelastic fluid.

We briefly outline the contents of this paper. At the end of this section we recapture some of the modelling aspects of isothermal viscoelastic flow. Section 2 is devoted to a description of the non-isothermal viscoelastic model that we shall employ. A description of the thermal optimal control problem is given in section 3, as well as a first order necessary optimality condition which will be the basis for the numerical realization of the optimal control. A description of the numerical treatment of the optimal control problem is presented in Section 4. The last section finally contains selected numerical results. The Appendix **A** is devoted to the derivation of the adjont system and the optimality condition.

The equations which rule the flow of fluids are the momentum and the mass balance equations, which for incompressible flow are given by

$$\rho \frac{dU}{dt} = \text{ Div } \boldsymbol{\sigma} + \rho f \tag{1.1}$$

$$\text{div } U = 0 \quad , \tag{1.2}$$

where U is the velocity, $\frac{dU}{dt}$ its material derivative, $\boldsymbol{\sigma}$ is the stress tensor, ρ is the mass density, ρf represents the body forces and Div $\boldsymbol{\sigma} = \begin{pmatrix} \sigma_{xx,x} + \sigma_{xy,y} \\ \sigma_{xy,x} + \sigma_{yy,y} \end{pmatrix}$. The stress tensor $\boldsymbol{\sigma}$

has the form

$$\boldsymbol{\sigma} = -p\mathbf{I} + \boldsymbol{\tau} \tag{1.3}$$

where p denotes the pressure, $\mathbf{I}$ the unit tensor and $\boldsymbol{\tau}$ stands for the so-called extra-stress tensor. For a viscoelastic fluid, the simplest model is the isothermal Oldroyd-B model[21], which relates the extra-stress $\boldsymbol{\tau}$ to the kinetics :

$$\boldsymbol{\tau} + \lambda \frac{\mathcal{D}\boldsymbol{\tau}}{\mathcal{D}t} = 2\eta[\ \mathbf{D} + \lambda_r \frac{\mathcal{D}\mathbf{D}}{\mathcal{D}t}\ ] \quad , \tag{1.4}$$

where $\frac{\mathcal{D}\boldsymbol{\tau}}{\mathcal{D}t}$ is the upper convected objective derivative of $\boldsymbol{\tau}$. Here λ denotes the relaxation time of the fluid, η its viscosity, $0 \leq \lambda_r < \lambda$ its retardation time, and $\mathbf{D}$ is the rate of deformation tensor ($\mathbf{D} = \frac{1}{2}(\nabla U + \nabla U^T)$). The term $\lambda_r \frac{\mathcal{D}\mathbf{D}}{\mathcal{D}t}$ suggests that the non-Newtonian fluid is constituted by a solvent part (Newtonian fluid) whose contribution to the total extra-stress is $\boldsymbol{\tau}_S$, and a polymeric part with stress $\boldsymbol{\tau}_P$:

$$\boldsymbol{\tau} = \boldsymbol{\tau}_S + \boldsymbol{\tau}_P \quad , \tag{1.5}$$

with

$$\boldsymbol{\tau}_S = 2\eta_S \mathbf{D} \qquad \text{and} \qquad \eta = \eta_S + \eta_P \quad . \tag{1.6}$$

The resulting equation for $\boldsymbol{\tau}_P$ is found to be

$$\boldsymbol{\tau}_P + \lambda\ \frac{\mathcal{D}\boldsymbol{\tau}_P}{\mathcal{D}t} = 2\eta_P \mathbf{D} \quad , \tag{1.7}$$

with $\eta_P = \eta(1 - \frac{\lambda_r}{\lambda})$. It is well known that the predictions of the Oldroyd-B model for viscometric flows has some shortcomings. Failures also occur in numerical simulations for high Weissenberg numbers which is the non dimensional number that quantifies the elasticity of the fluid.

The linearised Phan-Tien-Tanner (PTT) model [26] partially avoids these difficulties. Compared to the Oldroyd-B model, it contains a non linear term involving $\boldsymbol{\tau}_P$ and a positive parameter ϵ related to the elongational behaviour of the fluid, which tends to lower the stresses :

$$\boldsymbol{\tau}_P + \lambda \frac{\mathcal{D}\boldsymbol{\tau}_P}{\mathcal{D}t} + \epsilon \frac{\lambda}{\eta_P} \mathrm{Tr}(\boldsymbol{\tau}_P)\boldsymbol{\tau}_P = 2\eta_P \mathbf{D} \quad . \tag{1.8}$$

The non-isothermal constitutive equation that we shall utilize will be based on the PTT model where we allow the relaxation time λ and the polymer viscosity η_P to depend on the temperature.

2 Non-isothermal fluids

Let us first recall that the physical parameters in the isothermal model described by (1.1)-(1.3) and (1.6)-(1.8) are given by the solvent viscosity η_S, the polymeric viscosity η_P, the relaxation time λ, and ρ the density, while k and C_p the heat diffusion coefficient and the capacity are the physical parameters which appear in the energy equation (see next paragraph). For non-isothermal models, k and C_p are commonly considered to be independent of T. We choose also ρ as a constant, and allow η_S, η_P and λ to depend on temperature.

2.1 Energy equation

For viscous flows, the usual energy balance equation is :

$$\rho \frac{de}{dt} = -\text{div}\ q + \boldsymbol{\tau} : \mathbf{D} \quad , \tag{2.1}$$

where e is the specific internal energy and q the heat flux, and ρ the mass density. Assuming that the internal energy e is only function of the temperature, we obtain :

$$\frac{de}{dt} = \frac{\partial e}{\partial T}\ \frac{dT}{dt} = C_p\ \frac{dT}{dt} \quad , \tag{2.2}$$

where C_p denotes the thermal capacity.The heat flux follows the Fourier's law :

$$q = -k \nabla T \quad , \tag{2.3}$$

with k the thermal conductivity. Finally, the energy balance reduces to

$$\rho C_p \frac{dT}{dt} = k \Delta T + \boldsymbol{\tau} : \mathbf{D} \quad . \tag{2.4}$$

Since a viscoelastic fluid can store energy thanks to its elastic behaviour, the latter equation has to be modified [22]. For the PTT model, the energy equation is

$$\rho C_p \frac{dT}{dt} = k \Delta T + \kappa(\boldsymbol{\tau} : \mathbf{D}) + (1-\kappa) \frac{\text{Tr}(\boldsymbol{\tau})}{2\lambda} \quad , \tag{2.5}$$

with $0 \leq \kappa \leq 1$. The case $\kappa = 1$ corresponds to a pure entropy elasticity, $\kappa = 0$ corresponds to a pure energy elasticity.

2.2 Modelling of non-isothermal viscoelastic fluids

Many authors have proposed different models to describe non-isothermal viscoelastic fluids [4][6][12][17][18][22] [23][24][25][28][29][30] We give a brief summary of interesting approach before we focus on the model that we shall utilize.
Phan-Thien [23] derives from the dumbbells model a "non-isothermal Oldroyd-B" model, which differs from its isothermal counterpart. The new constitutive equation is

$$\boldsymbol{\tau}_P + \lambda(T)[\frac{\mathcal{D}\boldsymbol{\tau}_P}{\mathcal{D}t} - \boldsymbol{\tau} \cdot \frac{\text{d}lnT}{\text{d}t}] = 2\eta_P(T)\mathbf{D} \quad , \tag{2.6}$$

with the laws for $\eta_S(T)$ and $\eta_P(T)$ given by

$$\eta_S(T) = \eta_S(T_0)\ \exp[-\alpha(T-T_0)] \quad , \tag{2.7}$$

$$\eta_P(T) = \eta_P(T_0)\ \exp[-\alpha(T-T_0)] \quad . \tag{2.8}$$

The law for the relaxation time is chosen to be

$$\lambda(T) = \lambda(T_0)\ \frac{T_0}{T}\ \exp[-\alpha(T-T_0)] \quad . \tag{2.9}$$

The constitutive equation (2.6) is used [25] to solve the extrudate-swell problem. In order to reach higher Weissenberg numbers, the authors utilize a "non-isothermal PTT model", obtained by adding the term $\epsilon \frac{\mathrm{We}(T)}{\eta_P(T)} \mathrm{Tr}(\boldsymbol{\tau}_P)\boldsymbol{\tau}_P$ to the left hand side of (2.6). In [18] the authors also considered an integral model of Papanastasiou type to solve the same extrusion problem, with the use of a pseudo time and the shift factor a_T in the integral form of the constitutive equation. A more general version of constitutive equation is given in [12].

In a more recent work, for the simulation of the flow around a sphere, Peters et al. [22] use a Maxwell model (no solvent viscosity) and the PTT model (1.8) together with the WLF model for the temperature dependency of the physical parameters (relaxation time λ and polymeric viscosity η_P) :

$$\lambda(T) = \lambda(T_0)\ f(T) \quad , \tag{2.10}$$
$$\eta_P(T) = \eta_P(T_0)\ f(T) \tag{2.11}$$

where f is given by

$$f(T) = \exp[-\frac{c_1 \cdot (T - T_0)}{c_2 + (T - T_0)}\ ] \quad , \tag{2.12}$$

and T_0 a reference temperature. If T_0 is near the glass transition temperature, viscosity and relaxation time vary significantly with T. In this case the parameters $(c_1; c_2)$ are $(15; 50)$. Far from the glass transition $(c_1; c_2) = (5; 150)$: temperature has small effects on viscosity and relaxation time. This is illustrated in the following plot (Figure 1). In the present

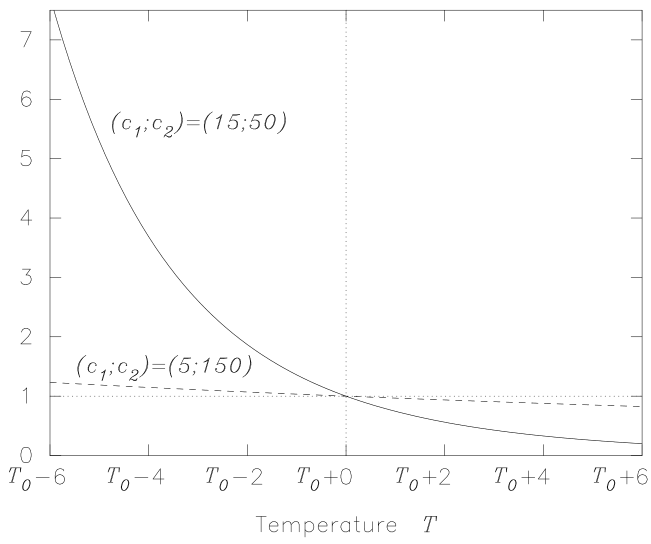

Fig 1: WLF function for two sets of parameters

work, we suppose that the viscoelastic fluid contains a solvent part. We have to give the solvent viscosity as a function of T, i.e. we choose $\eta_S(T) = \eta_S(T_0) f_s(T)$ with a proper choice of f_s. Since the solvent is a low-molecular fluid, its viscosity follows the laws for such fluids [2], and we set :

$$\eta_S(T) = \eta_S(T_0)\ \exp(-\beta T) \quad . \tag{2.13}$$

Our model for non-isothermal fluids utilizes the PTT model (1.8) together with (2.10)-(2.13) for the description of the temperature dependency. We prefer this approach over the non-isothermal Oldroyd-B (or PTT) with (2.7)-(2.9) model since the flow appears to be well described and it simplifies the primal system as well as the dual system which will be derived for the control problem.

Henceforth we shall simplify our notations : $\boldsymbol{\tau}$ stands for $\boldsymbol{\tau}_P$, λ for $\lambda(T_0)$ so that $\lambda(T) = \lambda\ f(T)$ and analogously $\eta_P(T) = \eta\ f(T)$ and $\eta_S(T) = \eta_S.\exp(-\beta T)$.

Finally, the system describing the non isothermal fluid that we utilize is given by

$$(NIF)\begin{cases} \rho(\ \dfrac{\partial U}{\partial t} + (U\cdot\nabla)U\ ) = -\nabla p + \ \eta_S(T)\Delta U + \mathrm{Div}\ \boldsymbol{\tau} \\ \\ \mathrm{div}\ U = 0 \\ \\ \lambda(T)\dfrac{\mathcal{D}\boldsymbol{\tau}}{\mathcal{D}t} + [1+\epsilon\dfrac{\lambda(T)}{\eta_P(T)}Tr(\boldsymbol{\tau})]\boldsymbol{\tau} = 2\eta_P(T)\ \mathbf{D} \\ \\ \rho C_p(\ \dfrac{\partial T}{\partial t} + (U\cdot\nabla)T\ ) = k\Delta T + \kappa(\boldsymbol{\tau}:\mathbf{D}) + (1-\kappa)\dfrac{\mathrm{Tr}(\boldsymbol{\tau})}{2\lambda(T)} \quad . \end{cases}$$

2.3 Dimensionless equations

We define the dimensionless variables (with stars) :

$$X^* = \frac{X}{L}\ , \qquad U^* = \frac{U}{U_0}\ , \qquad p^* = \frac{pL}{\eta_0 U_0}\ , \qquad T^* = \frac{T-T_0}{T_w - T_0}$$

$$\boldsymbol{\tau}^* = \frac{\boldsymbol{\tau} L}{\eta_0 U_0}\ , \qquad t^* = \frac{tU_0}{L}\ .$$

Here L is the characteristic dimension of the domain, U_0 the characteristic velocity, T_0 the reference temperature, T_w the wall temperature, and η_0 is the total stress at $T = T_0$. We introduce also the following characteristic numbers :

- The Reynolds number : $\mathrm{Re} = \rho\ \dfrac{U_0 L}{\eta_0}$.
- The Weissenberg number : $\mathrm{We} = \lambda\ \dfrac{U_0}{L}$.
- A retardation parameter ω_r in]0:1[equal to $\omega_r = 1 - \dfrac{\lambda_r}{\lambda}$
- The Prandtl number : $\mathrm{Pr} = \dfrac{\nu}{\alpha} = \dfrac{C_p \eta}{k}$
- The Peclet number $\mathrm{Pe} = \dfrac{U_0 L}{\alpha}$ (Pe = Pr .Re)
- The Brinkman number $\mathrm{Br} = \dfrac{\eta\ U_0^2}{k(T_w - T_0)}$.

The Peclet number describes the ratio of heat convection to heat conduction. For injection moulding, it is typically between 100 and 1000. The Brinkman number represents the ratio of viscous dissipation to heat conduction resulting from imposed temperature difference, ie the importance of self-heating versus external heating.

We consider first the function of the WLF model (2.12). Replacing in this expression T by T^* gives the non-dimensional function f^* for the non-dimensional temperature T^*:

$$f^*(T^*) = \exp[-\frac{c_1 \cdot T^*}{c_2/(T_w - T_0) + T^*}\ ] \tag{2.14}$$

As we do not know a priori which temperature will be imposed on the wall in the course of the control problem, we set the quantity $T_w - T_0 = 1$. It will turn out that we will obtain a control temperature of reasonable order of magnitude. In the following we put $\mathrm{We}(T^*) = \mathrm{We}.f^*(T^*)$, $\omega_r(T^*) = \omega_r\ .f^*(T^*)$, and $(1-\omega_r)(T)$ the non-dimensional solvent viscosity function of T. Dropping there-forth the notation $\ ^*$ for the non-dimensional variables we obtain the following system in non-dimensional coordinates :

$$(S)\quad \begin{cases} \mathrm{Re}[\ \dfrac{\partial U}{\partial t} + (U\cdot\nabla)\ U\ ] = -\nabla p + (1-\omega_r)(T)\Delta U + \mathrm{Div}\ \boldsymbol{\tau} \\[2ex] \mathrm{div}\ U = 0 \\[2ex] \mathrm{We}(T)\dfrac{\mathcal{D}\boldsymbol{\tau}}{\mathcal{D}t} + [1+\epsilon\dfrac{\mathrm{We}(T)}{\omega_r(T)}\mathrm{Tr}(\boldsymbol{\tau})]\boldsymbol{\tau} = 2\omega_r(T)\mathbf{D} \\[2ex] \dfrac{\partial T}{\partial t} + (U\cdot\nabla)\ T = \dfrac{1}{\mathrm{Pe}}[\Delta T + \mathrm{Br}[\ \kappa(\boldsymbol{\tau}:\mathbf{D}) + (1-\kappa)\dfrac{\mathrm{Tr}(\boldsymbol{\tau})}{2\mathrm{We}(T)}\ ]\ ]\quad . \end{cases}$$

2.4 Model simplification

Within this paper, we consider control of steady state flows, so that all the transient terms are neglected. As we want to act on the fluid by strongly cooling or heating the wall, the Brinkman number is small, and therefore the term of self heating will be neglected.
Another simplification is made : we set the Newtonian viscosity independent of temperature. Although this may be a poor approximation in "real world", we believe that it has only a minor influence on our computed solutions. For an exhaustive review of model simplification, see [27]. Finally, we note that the Weissenberg number and the polymeric viscosity have the same functional temperature dependency, thus $\dfrac{\mathrm{We}(T)}{\eta_P(T)} = \dfrac{\mathrm{We}}{\eta_P}$. The system to be solved is therefore given by :

$$(P)\quad \begin{cases} \mathrm{Re}[\ (U\cdot\nabla)\ U\ ] = -\nabla p + (1-\omega_r)\Delta U + \mathrm{Div}\ \boldsymbol{\tau} \\[2ex] \mathrm{div}\ U = 0 \\[2ex] \mathrm{We}(T)[\ (U\cdot\nabla)\ \boldsymbol{\tau} - \nabla U\cdot\boldsymbol{\tau} - \boldsymbol{\tau}\cdot\nabla U^T\ ] + [1+\epsilon\dfrac{\mathrm{We}}{\omega_r}\mathrm{Tr}(\boldsymbol{\tau})]\boldsymbol{\tau} = 2\omega_r(T)\mathbf{D} \\[2ex] (U\cdot\nabla)\ T = \dfrac{1}{\mathrm{Pe}}\Delta T\quad . \end{cases}$$

This system has to be completed with appropriate boundary conditions.

2.5 Boundary conditions

We suppose non-slip boundary conditions for the wall velocities. At the inflow and outflow, we impose Dirichlet conditions obtain from a fully developed Poiseuille flow. Since the equation for $\boldsymbol{\tau}$ is of transport type boundary conditions are given only at the inflow. Again we use boundary conditions corresponding to a Poiseuille flow. For the temperature, we set $T = 0$ at the inflow. Thus we neglect the heat that could be produced by self-heating of the fluid before it reaches the contraction (see [23] for other boundary condition at the inflow). Concerning the thermal boundary conditions on the wall, homogenous Neumann boundary conditions are chosen on the uncontrolled parts and Dirichlet conditions are imposed on those parts of the wall where a control $\mathbf{g}$ is enforced. This results in the following set of boundary conditions (B.C) :

$$
(BC)\left\{\begin{array}{llll}
U = U_{in} & \text{on } \Gamma_{in}\ , & U = U_{out} & \text{on } \Gamma_{out} \\
U = 0 & \text{elsewhere} & & \\
 & & & \\
\boldsymbol{\tau} = \boldsymbol{\tau}_{in} & \text{on } \Gamma_{in} & & \\
 & & & \\
T = 0 & \text{on } \Gamma_{in}\ , & T = \mathbf{g} & \text{on } \Gamma_c \\
\dfrac{\partial T}{\partial n} = 0 & \text{on } \Gamma_n = \Gamma \setminus (\Gamma_{in} \cup \Gamma_c). & &
\end{array}\right.
$$

3 The optimal control problem

In this section we formulate the open loop optimal control problem and a first order necessary optimality condition. The optimal control problem consists in minimizing a functional $\mathcal{J}$ depending on the velocity field U and the boundary control $\mathbf{g}$. The system (P) together with the boundary conditions (BC) will arise as constraints in the optimal control problem. For the convenience of the reader we summerize those equations in the following problem statement :

$(\mathcal{P})$: Minimize $\mathcal{J}(U, \mathbf{g})$ subject to :

$$
(P)\quad\left\{\begin{array}{l}
\mathrm{Re}[\ (U\cdot\nabla)\ U\ ] = -\nabla p + (1-\omega_r)\Delta U + \mathrm{Div}\ \boldsymbol{\tau} \\
 \\
\mathrm{div}\ U = 0 \\
 \\
\mathrm{We}(T)[\ (U\cdot\nabla)\ \boldsymbol{\tau} - \nabla U\cdot\boldsymbol{\tau} - \boldsymbol{\tau}\cdot\nabla U^T\ ] + [1+\epsilon\dfrac{\mathrm{We}}{\omega_r}\mathrm{Tr}(\boldsymbol{\tau})]\boldsymbol{\tau} = 2\omega_r(T)\mathbf{D} \\
 \\
(U\cdot\nabla)\ T = \dfrac{1}{\mathrm{Pe}}\Delta T \quad .
\end{array}\right.
$$

$$
(BC)\left\{\begin{array}{llll}
U = U_{in} & \text{on } \Gamma_{in}\ , & U = U_{out} & \text{on } \Gamma_{out} \\
U = 0 & \text{elsewhere} & & \\
 & & & \\
\boldsymbol{\tau} = \boldsymbol{\tau}_{in} & \text{on } \Gamma_{in} & & \\
 & & & \\
T = 0 & \text{on } \Gamma_{in}\ , & T = \mathbf{g} & \text{on } \Gamma_c \\
\dfrac{\partial T}{\partial n} = 0 & \text{on } \Gamma_n = \Gamma \setminus (\Gamma_{in} \cup \Gamma_c). & &
\end{array}\right.
$$

In the numerical examples Ω is chosen as the suddenly contracting channel as depicted in Figure 2 (the figure also contains the boundary conditions and the domain of observation $\tilde{\Omega}$). The cost $\mathcal{J}$ is chosen such that the controlled flow has a small recirculation zone

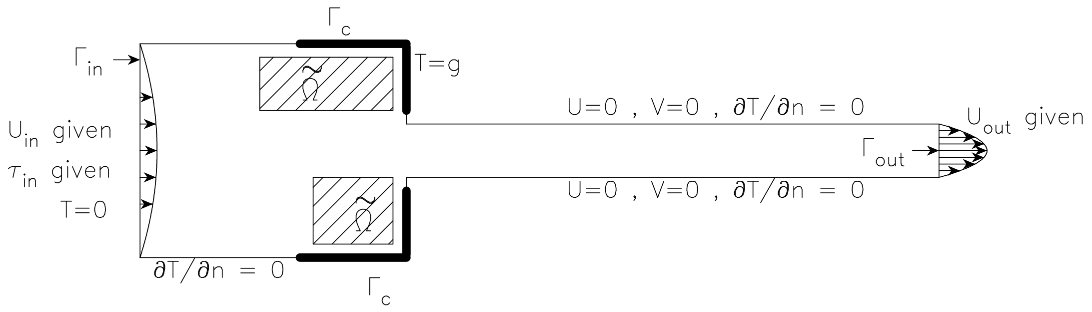

Fig 2: Domain of the flow

and the flow there has a lower energy than the uncontrolled flow. There is no unique best choice for $\mathcal{J}$ to achieve this goal. It is our experience with optimal control problems for the Navier-Stokes equations, for example, that the value of the cost at the solution can have a significant impact on the success of numerical minimizing routine or lack thereof. This is related to the second order sufficient optimality condition which is more likely to be satisfied for small than for large residue problem.
With these comments in mind we choose two types of cost functionals :

$$
\mathcal{J}_1(U,\mathbf{g}) \;=\; \frac{\alpha}{2}\int_{\tilde{\Omega}} |U - U_{ns}|^2 \, dx \;+\; \frac{\gamma}{2}\int_{\Gamma_c} |\mathbf{g}|^2 \, dx \quad , \tag{3.1}
$$

$$
\mathcal{J}_2(U,\mathbf{g}) \;=\; \frac{\alpha}{2}\int_{\tilde{\Omega}} |\mathrm{Min}(0,u)|^2 \, dx \;+\; \frac{\gamma}{2}\int_{\Gamma_c} |\mathbf{g}|^2 \, dx \quad , \tag{3.2}
$$

where α and γ specify the cost of the state and control, $\tilde{\Omega} \in \Omega$ denotes the observation region, U_{ns} stands for the solution of the velocity field of the Newtonian fluid with the same boundary conditions as in (BC), which is known to have a smaller recirculation zone than the non-Newtonian fluid, and $U = (u, v)$. The functional $\mathcal{J}_1$ is of tracking type : the thermal control has to be chosen such that the controlled non-Newtonian fluid behaves "almost like" a Newtonian one. $\mathcal{J}_2$ on the other hand penalizes negative contributions to the flow component in the longitudinal direction of the channel.
Let us henceforth denote by $\mathbf{g}^\star$ an optimal control, i.e. a solution to $(\mathcal{P})$, and let $(\ U^\star, p^\star, \boldsymbol{\tau}^\star, T^\star\ ) = (\ U(\mathbf{g}^\star), p(\mathbf{g}^\star), \boldsymbol{\tau}(\mathbf{g}^\star), T(\mathbf{g}^\star)\ )$. Then $(\ U^\star, p^\star, \boldsymbol{\tau}^\star, T^\star\ )$ must satisfy the primal equation, i.e.

(P) and (BC), the dual system (D) in terms of the dual variables $(\xi, \pi, \boldsymbol{\theta}, \rho)$ corresponding to $(U, p, \boldsymbol{\tau}, T)$ as well as the optimality condition (OC) :

Dual system :

$$
(D) \left\{ \begin{array}{l}
\mathrm{Re}\ [\ -(U\cdot\nabla)\xi + \nabla U^T \cdot \xi\ ] - (1-\omega_r)\Delta\xi - \nabla\pi = \ -\mathcal{J}_U \\
\qquad\qquad\qquad - 2\frac{\omega_r}{\mathrm{We}}\mathrm{Div}\ \boldsymbol{\theta}\ -\ \left(\begin{array}{c} \partial_x\boldsymbol{\tau} : \boldsymbol{\theta} \\ \partial_y\boldsymbol{\tau} : \boldsymbol{\theta} \end{array}\right) - 2\ \mathrm{Div}\ (\boldsymbol{\theta}\boldsymbol{\tau})\ -\ \rho\ \nabla T\ \ , \\
\mathrm{div}\ \xi = 0 \quad , \\
\mathrm{We}(T)[\ -(U\cdot\nabla)\boldsymbol{\theta} - \boldsymbol{\theta}\cdot\nabla U - \nabla U^T\cdot\boldsymbol{\theta}\ ]\ + \boldsymbol{\theta}\ +\ \epsilon\frac{\mathrm{We}}{\omega_r}[\mathrm{Tr}(\boldsymbol{\tau})\boldsymbol{\theta} + (\boldsymbol{\tau}:\boldsymbol{\theta})\mathbf{I}] = -\mathrm{We}(T).\mathbf{D}(\xi)\ \ , \\
-\ (U\cdot\nabla)\rho\ -\ \frac{1}{\mathrm{Pe}}\Delta\rho\ +\ (\frac{1}{\mathrm{We}})'(T)[1+\epsilon\frac{\mathrm{We}}{\omega_r}\mathrm{Tr}(\boldsymbol{\tau})]\boldsymbol{\tau}:\boldsymbol{\theta} = 0\ \ , \\
\text{boundary conditions :} \\
\quad \xi = 0 \text{ on } \Gamma \\
\quad \boldsymbol{\theta} = 0 \text{ on } \Gamma_{out} \\
\quad \rho = 0 \text{ on } \Gamma_{in}\cup\Gamma_c\ ;\ \frac{1}{\mathrm{Pe}}\partial_n\rho = -u\rho \text{ on } \Gamma_{out}\ ;\ \partial_n\rho = 0 \text{ on } \Gamma\setminus(\Gamma_{in}\cup\Gamma_c\cup\Gamma_{out})\ \ ,
\end{array}\right.
$$

Optimality condition :

$$
\text{(OC)} \qquad \gamma.\mathbf{g} = -\frac{1}{\mathrm{Pe}}\partial_n\rho \quad \text{on } \Gamma_c \quad . \tag{3.3}
$$

Above $\chi_{\tilde{\Omega}}$ denotes the characteristic function of the sub-domain $\tilde{\Omega}$, i.e. $\chi_{\tilde{\Omega}} = 1$ if $x \in \tilde{\Omega}$ and $= 0$ otherwise, and $\mathcal{J}_U$ stands for the directional derivative of $\mathcal{J}$ with respect to U. For $\mathcal{J}_1$ and $\mathcal{J}_2$ we find

$$
\mathcal{J}_{1,U} = \alpha\ (U - U_{ns})\ \chi_{\tilde{\Omega}} \quad \text{and} \quad \mathcal{J}_{2,U} = \alpha\ (\mathrm{Min}(0,u),0)\ \chi_{\tilde{\Omega}} \tag{3.4}
$$

A formal derivation of the optimality system is given in the Appendix **A**.

4 Solution method

4.1 The staggered grids, notation

The discretisation of the unknowns is carried out on the non-uniform grid depicted in Figure 3.

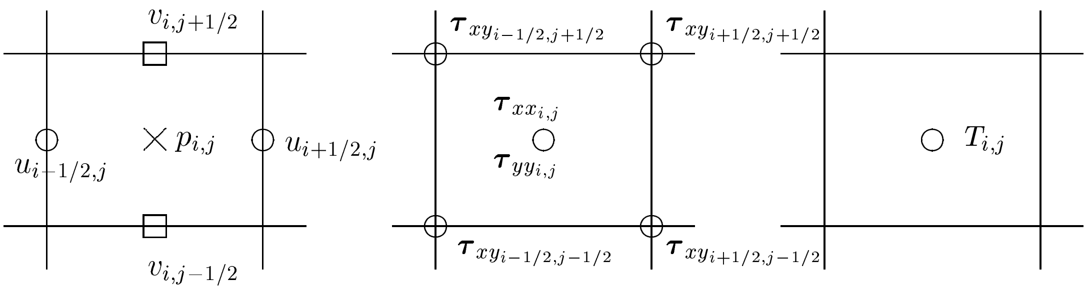

Fig 3 : Discretization of the unknowns

For the variables of the adjoint equation the same locations are used. This staggered grid is classical for the resolution of the Navier-Stokes equations, and the location of the temperature at the center of the cells is also usual. Concerning the three unknowns for the stress $\boldsymbol{\tau}_{xx}$, $\boldsymbol{\tau}_{yy}$ and $\boldsymbol{\tau}_{xy}$, their locations allow us, as we shall see, to simplify in a certain manner the discretisation of the equations. We will also have to use the values of all the unknowns at points different from their nodes. Concerning u and v, we define the value $\tilde{u}_{i,j-1/2}$ as the value of u at the node of v, and $\tilde{v}_{i-1/2,j}$, the value of v, at the node of u. This is achieved with bilinear interpolation of the four nearest neighbours of u and v, as shown on Figure 4 :

$$\tilde{u}_{i,j-1/2} = b_1 u_{i-1/2,j-1} + b_2 u_{i+1/2,j-1} + b_3 u_{i-1/2,j} + b_4 u_{i+1/2,j} \tag{4.1}$$

$$\tilde{v}_{i,j-1/2} = c_1 v_{i-1,j-1/2} + c_2 v_{i-1,j-1/2} + c_3 v_{i,j+1/2} + c_4 v_{i,j+1/2} \quad . \tag{4.2}$$

Let us define the distances Δx_i, Δy_j, $\Delta x_{i-1/2}$, $\Delta y_{j-1/2}$ according to Figure 4. Then the calculation of the coefficients $b_1, \dots, b_4$ and $c_1, \dots, c_4$ is straightforward. In a similar

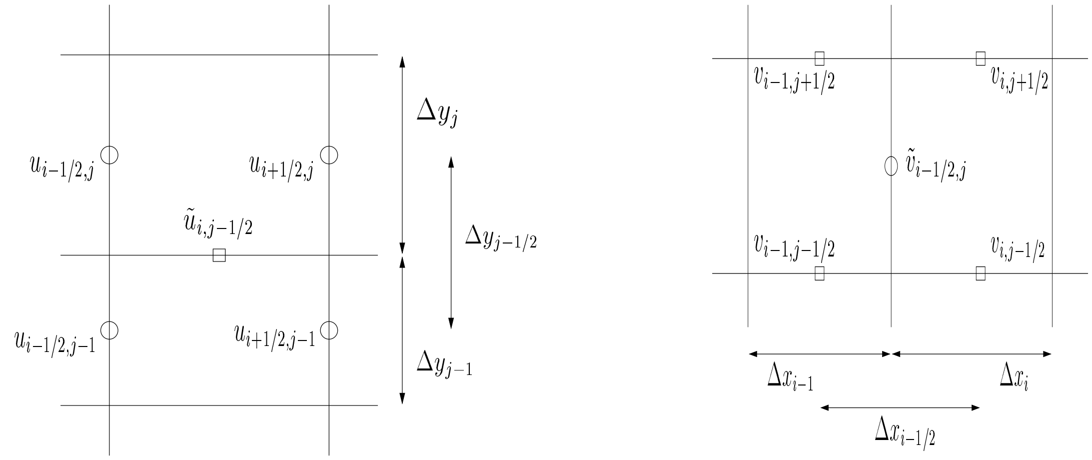

Fig 4: Interpolation of u at the node of v and interpolation of v at the node of u

manner, we introduce $\tilde{\boldsymbol{\tau}}_{xx_{i-1/2,j-1/2}}$, $\tilde{\boldsymbol{\tau}}_{yy_{i-1/2,j-1/2}}$ and $\tilde{T}_{i-1/2,j-1/2}$ as the interpolated values of $\boldsymbol{\tau}_{xx}$, $\boldsymbol{\tau}_{yy}$ and T at the node for $\boldsymbol{\tau}_{xy_{i-1/2,j-1/2}}$, and $\tilde{\boldsymbol{\tau}}_{xy_{i,j}}$ which is the interpolated value of $\boldsymbol{\tau}_{xy}$ at the node for $\boldsymbol{\tau}_{xx_{i,j}}$ (see Fig 5). This is again achieved by bilinear interpolation as follows :

$$\begin{aligned}
\tilde{\boldsymbol{\tau}}_{xx_{i-1/2,j-1/2}} &= d_1 \boldsymbol{\tau}_{xx_{i-1,j-1}} + d_2 \boldsymbol{\tau}_{xx_{i-1,j}} + d_3 \boldsymbol{\tau}_{xx_{i,j-1}} + d_4 \boldsymbol{\tau}_{xx_{i+1,j+1}} &(4.3)\\
\tilde{\boldsymbol{\tau}}_{yy_{i-1/2,j-1/2}} &= d_1 \boldsymbol{\tau}_{yy_{i-1,j-1}} + d_2 \boldsymbol{\tau}_{yy_{i-1,j}} + d_3 \boldsymbol{\tau}_{yy_{i,j-1}} + d_4 \boldsymbol{\tau}_{yy_{i+1,j+1}} &(4.4)\\
\tilde{T}_{i-1/2,j-1/2} &= d_1 T_{i-1,j-1} + d_2 T_{i-1,j} + d_3 T_{i,j-1} + d_4 T_{i+1,j+1} &(4.5)
\end{aligned}$$

$$\tilde{\boldsymbol{\tau}}_{xy_{i-1,j-1}} = e_1 \boldsymbol{\tau}_{xy_{i-1/2,j-1/2}} + e_2 \boldsymbol{\tau}_{xy_{i-1/2,j+1/2}} + e_3 \boldsymbol{\tau}_{xy_{i+1/2,j-1/2}} + e_4 \boldsymbol{\tau}_{xy_{i+1/2,j+1/2}} \quad . \tag{4.6}$$

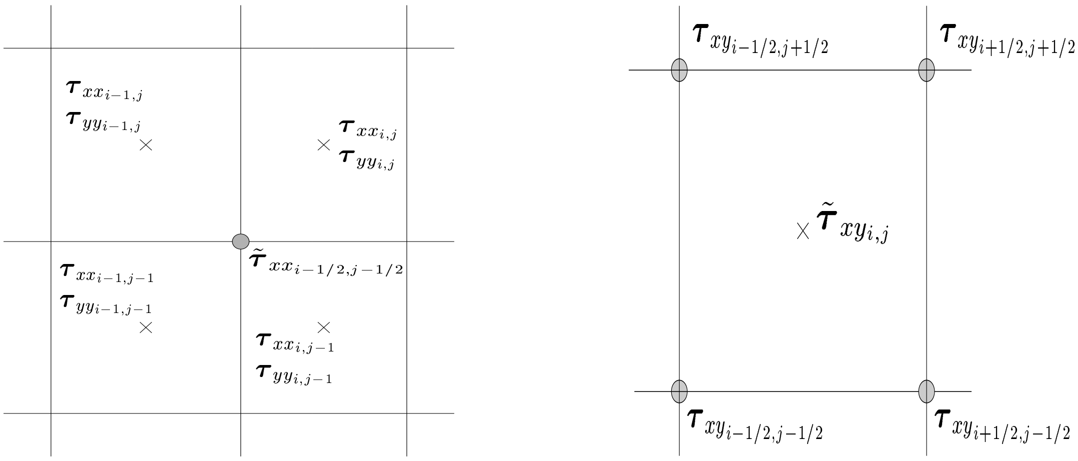

Fig 5: Interpolation of $\boldsymbol{\tau}_{xx}$ or $\boldsymbol{\tau}_{yy}$ at the node of $\boldsymbol{\tau}_{xy}$ and Interpolation of $\boldsymbol{\tau}_{xy}$ at the node of $\boldsymbol{\tau}_{xx}$

4.2 Discretisation of the equations - primal system

• **Heat equation :**

$$(U \cdot \nabla)\, T = \frac{1}{\mathrm{Pe}} \Delta T \quad . \tag{4.7}$$

At the points of index (i, j), the Laplacian is discretized by be usual 5 points scheme:

$$\Delta T \;\rightarrow -a_{i,j} T_{i,j} + a_{i-1,j} T_{i-1,j} + a_{i+1,j} T_{i+1,j} + a_{i,j-1} T_{i,j-1} + a_{i,j+1} T_{i,j+1} \quad . \tag{4.8}$$

The calculus for the coefficient $a_{i-1,j}, a_{i,j}, a_{i+1}, a_{i,j-1}, a_{i,j+1}$ is straightforward. The convection term is discretized following the upwind scheme :

$$u \frac{\partial T}{\partial x} \rightarrow \begin{cases} u_{i-1/2,j} \dfrac{T_{i,j} - T_{i-1,j}}{\Delta x_{i-1/2}} & \text{if } u_{i-1/2,j} > 0 \text{ and } (u_{i+1/2,j} > 0 \text{ or } |u_{i-1/2,j}| > |u_{i+1/2,j}|) \\ u_{i+1/2,j} \dfrac{T_{i+1,j} - T_{i,j}}{\Delta x_{i+1/2}} & \text{if } u_{i+1/2,j} < 0 \text{ and } (u_{i-1/2,j} < 0 \text{ or } |u_{i+1/2,j}| > |u_{i-1/2,j}|) \\ 0 & \text{elsewhere} \quad , \end{cases} \tag{4.9}$$

and similarly

$$v \frac{\partial T}{\partial y} \rightarrow \begin{cases} v_{i,j-1/2} \dfrac{T_{i,j} - T_{i,j-1}}{\Delta y_{j-1/2}} & \text{if } v_{i,j-1/2} > 0 \text{ and } (v_{i,j+1/2} > 0 \text{ or } |v_{i,j-1/2}| > |v_{i,j+1/2}|) \\ v_{i,j+1/2} \dfrac{T_{i,j+1} - T_{i,j}}{\Delta y_{j+1/2}} & \text{if } v_{i,j+1/2} < 0 \text{ and } (v_{i,j+1/2} < 0 \text{ or } |v_{i,j+1/2}| > |v_{i,j-1/2}|) \\ 0 & \text{elsewhere} \quad . \end{cases} \tag{4.10}$$

In (4.9) and (4.10) the choice for the upwinding strategy is motivated by the special situation that occurs if a flow component is directed towards a node from either side, as $u_{i-1/2,j} > 0$ and $u_{i+1/2,j} < 0$ for instance. In this case, the decision is made by considering the higher absolute value of these two quantities.

If we are at a point near the boundary with homogenous Neumann conditions (i.e. on $\partial\Omega \setminus (\Gamma_c \cup \Gamma_{in})$) as in Figure 6 on the horizontal wall for example , we set

$$T_{i,0} = T_{i,1} \tag{4.11}$$

and apply at the points of index $(i,1)$ the same discretisation as for interior points. If the

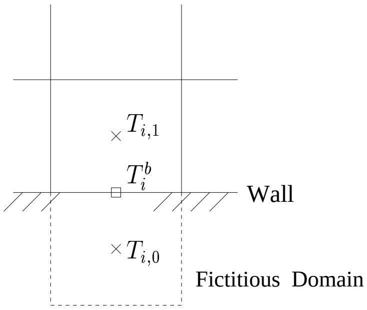

Fig 6: Homogeneous Neumann boundary condition - Fictitious domain

boundary condition is of Dirichlet type, $T_{i,0}$ is given by a quadratic extrapolation between $T_{i,2}$, $T_{i,1}$ and T_i^b. We employ the same technique for vertical walls.

- **Stress equation :**

$$\mathrm{We}(T)[\ (U\cdot\nabla)\ \boldsymbol{\tau} - \nabla U\cdot\boldsymbol{\tau} - \boldsymbol{\tau}\cdot\nabla U^T\ ] + [1+\epsilon\frac{\mathrm{We}}{\omega_r}\mathrm{Tr}(\boldsymbol{\tau})]\boldsymbol{\tau} = 2\omega_r(T)\mathbf{D}\ . \tag{4.12}$$

Concerning the two equations for $\boldsymbol{\tau}_{xx}$ and $\boldsymbol{\tau}_{yy}$ which are discretized at points of index (i,j), the evaluation of $\mathrm{We}(T)$ and $\omega_r(T)$ is immediate since the temperature is also defined at these points. The term $\mathrm{Tr}(\boldsymbol{\tau})$ presents also no difficulties.
The convective term $(U\cdot\nabla)\boldsymbol{\tau}$ is discretized in the same manner as used for the temperature scheme. The rate of deformation $\mathbf{D}$ is :

$$\mathbf{D} = \begin{pmatrix} u_x & (u_y+v_x)/2 \\ (u_y+v_x)/2 & v_y \end{pmatrix}\ , \tag{4.13}$$

so that its discretization is chosen as :

$$\text{eq. for } \boldsymbol{\tau}_{xx}: \quad (u_x)_{i,j} \to \frac{u_{i+1/2,j} - u_{i-1/2,j}}{\Delta x_i} \tag{4.14}$$

$$\text{eq. for } \boldsymbol{\tau}_{yy}: \quad (v_y)_{i,j} \to \frac{v_{i,j+1/2} - v_{i,j-1/2}}{\Delta y_j} \tag{4.15}$$

while in the equation for $\boldsymbol{\tau}_{xy}$, the component of $\mathbf{D}$ is discretized by :

$$(u_y+v_x)_{i-1/2,j-1/2} \to \frac{u_{i-1/2,j} - u_{i-1/2,j-1}}{\Delta y_{j-1/2}} + \frac{v_{i,j-1/2} - v_{i-1,j-1/2}}{\Delta x_{i-1/2}}\ . \tag{4.16}$$

Here the advantage of the locations of $\boldsymbol{\tau}_{xx}$, $\boldsymbol{\tau}_{yy}$ and $\boldsymbol{\tau}_{xy}$ clearly appears. Turning next to the discretization of the equation for $\boldsymbol{\tau}_{xy}$, the term $\mathrm{Tr}(\boldsymbol{\tau})$ is discretized by

$$\mathrm{Tr}(\boldsymbol{\tau})_{i-1/2,j-1/2} \to \tilde{\boldsymbol{\tau}}_{xx_{i-1/2,j-1/2}} + \tilde{\boldsymbol{\tau}}_{yy_{i-1/2,j-1/2}} \tag{4.17}$$

with the rules (4.3) and (4.4), and the temperature T at points of index $(i-\frac{1}{2}, j-\frac{1}{2})$ is computed according to the rule (4.5) :

$$(T)_{i-1/2,j-1/2} \to \tilde{T}_{i-1/2,j-1/2} \quad . \tag{4.18}$$

The convective term is discretized as for $\boldsymbol{\tau}_{xx}$ and $\boldsymbol{\tau}_{yy}$, except that we have utilized the values $\tilde{u}$ and $\tilde{v}$ for a correct upwinding :

$$(u.\boldsymbol{\tau}_{xy,x})_{i-1/2,j-1/2} \to \begin{cases} \tilde{u}_{i-1,j-1/2} \dfrac{\boldsymbol{\tau}_{xy_{i-1/2,j-1/2}} - \boldsymbol{\tau}_{xy_{i-3/2,j-1/2}}}{\Delta x_{i-1}} & \text{if } \tilde{u}_{i-1,j-1/2} > 0 \text{ and} \\ & (\tilde{u}_{i,j-1/2} > 0 \text{ or } |\tilde{u}_{i-,j-1/2}| > |\tilde{u}_{i,j-1/2}|) \\ \tilde{u}_{i,j-1/2} \dfrac{\boldsymbol{\tau}_{xy_{i+1/2,j-1/2}} - \boldsymbol{\tau}_{xy_{i-1/2,j-1/2}}}{\Delta x_i} & \text{if } \tilde{u}_{i,j-1/2} < 0 \text{ and} \\ & (\tilde{u}_{i-1,j-1/2} < 0 \text{ or } |\tilde{u}_{i,j-1/2}| > |\tilde{u}_{i-1,j-1/2}|) \\ 0 & \text{elsewhere} \quad , \end{cases} \tag{4.19}$$

and similarly

$$(v.\boldsymbol{\tau}_{xy,y})_{i-1/2,j-1/2} \to \begin{cases} \tilde{v}_{i-1/2,j-1} \dfrac{\boldsymbol{\tau}_{xy_{i-1/2,j-1/2}} - \boldsymbol{\tau}_{xy_{i-1/2,j-3/2}}}{\Delta y_{j-1}} & \text{if } \tilde{v}_{i-1/2,j-1} > 0 \text{ and} \\ & (\tilde{v}_{i-1/2,j} > 0 \text{ or } |\tilde{v}_{i-1/2,j-1}| > |\tilde{v}_{i-1/2,j}|) \\ \tilde{v}_{i-1/2,j} \dfrac{\boldsymbol{\tau}_{xy_{i-1/2,j+1/2}} - \boldsymbol{\tau}_{xy_{i-1/2,j-1/2}}}{\Delta y_j} & \text{if } \tilde{v}_{i-1/2,j} < 0 \text{ and} \\ & (\tilde{v}_{i-1/2,j-1} < 0 \text{ or } |\tilde{v}_{i-1/2,j}| > |\tilde{v}_{i-1/2,j-1}|) \\ 0 & \text{elsewhere} \quad . \end{cases} \tag{4.20}$$

Finally, with the term $\nabla U \cdot \boldsymbol{\tau} + \boldsymbol{\tau} \cdot \nabla U^T$, which is given by :

$$\nabla U \cdot \boldsymbol{\tau} + \boldsymbol{\tau} \cdot \nabla U^T = \begin{pmatrix} 2(u_x.\boldsymbol{\tau}_{xx} + u_y.\boldsymbol{\tau}_{xy}) & v_x.\boldsymbol{\tau}_{xx} + u_y.\boldsymbol{\tau}_{yy} \\ v_x.\boldsymbol{\tau}_{xx} + u_y.\boldsymbol{\tau}_{yy} & 2(v_x.\boldsymbol{\tau}_{xy} + v_y.\boldsymbol{\tau}_{yy}) \end{pmatrix} \quad ,$$

we proceed as follows :

eq. for $\boldsymbol{\tau}_{xx}$: u_x is given by centered differences (see (4.14))
u_y is evaluated by centered differences at node $(i-\dfrac{1}{2}, j-\dfrac{1}{2})$
and then by rule (4.6)
$\boldsymbol{\tau}_{xy}$ by rule (4.6) .

eq. for $\boldsymbol{\tau}_{yy}$: v_y is given by centered differences (see (4.15))
v_x is evaluated by centered differences at node $(i-\dfrac{1}{2}, j-\dfrac{1}{2})$
and then by rule (4.6)
$\boldsymbol{\tau}_{xy}$ by rule (4.6) .

eq. for $\boldsymbol{\tau}_{xy}$: v_x is given by centered differences
u_y is given by centered differences
$\boldsymbol{\tau}_{xx}$ and $\boldsymbol{\tau}_{yy}$ are given by rules (4.3)-(4.4) .

• **Momentum equation :**

$$\text{Re}[\ (U\cdot\nabla)\ U\ ] = -\nabla p + (1-\omega_r)\Delta U + \text{Div}\ \boldsymbol{\tau} \quad . \tag{4.21}$$

The discretisation of the Laplacian is discretized with the 5 points scheme.

$$\begin{aligned}
(\Delta u)_{i-1/2,j} \quad &\rightarrow \quad b_{i-3/2,j}.u_{i-3/2,j} \ - \ b_{i-1/2,j}.u_{i-1/2,j} \ + \ b_{i+1/2,j}.u_{i+1/2,j} \ + \\
&\qquad b_{i-1/2,j-1}.u_{i-1/2,j-1} \ + \ b_{i-1/2,j+1}.u_{i-1/2,j+1} \quad . &(4.22)\\
(\Delta v)_{i,j-1/2} \quad &\rightarrow \quad c_{i-1,j-1/2}.v_{i-1,j-1/2} \ - \ c_{i,j-1/2}.v_{i-1,j-1/2} \ + \ c_{i+1,j-1/2}.v_{i+1,j-1/2} \ + \\
&\qquad c_{i,j+1/2}.v_{i,j+1/2} \ + \ c_{i,j-3/2}.v_{i,j-3/2} \quad . &(4.23)
\end{aligned}$$

The discretisation of ∇p is immediate, due to the staggered grid :

$$\text{equation for } u : \qquad (p_x)_{i-1/2,j} \ \rightarrow \ \frac{p_{i,j}-p_{i-1,j}}{\Delta x_{i-1/2}} \tag{4.24}$$

$$\text{equation for } v : \qquad (p_y)_{i,j-1/2} \ \rightarrow \ \frac{p_{i,j}-p_{i,j-1}}{\Delta y_{j-1/2}} \quad . \tag{4.25}$$

The discretisation of the term Div $(\boldsymbol{\tau})$ is also easily made, once again due to our choice of localisation of the unknowns $\boldsymbol{\tau}$:

$$(\boldsymbol{\tau}_{xx,x})_{i-1/2,j} \ \rightarrow \ \frac{\boldsymbol{\tau}_{xx_{i,j}} - \boldsymbol{\tau}_{xx_{i-1,j}}}{\Delta x_{i-1/2}} \tag{4.26}$$

$$(\boldsymbol{\tau}_{xy,y})_{i-1/2,j} \ \rightarrow \ \frac{\boldsymbol{\tau}_{xy_{i-1/2,j+1/2}} - \boldsymbol{\tau}_{xy_{i-1/2,j-1/2}}}{\Delta y_j} \tag{4.27}$$

$$(\boldsymbol{\tau}_{xy,x})_{i,j-1/2} \ \rightarrow \ \frac{\boldsymbol{\tau}_{xy_{i+1/2,j-1/2}} - \boldsymbol{\tau}_{xy_{i-1.2,j-1/2}}}{\Delta x_i} \tag{4.28}$$

$$(\boldsymbol{\tau}_{yy,y})_{i,j-1/2} \ \rightarrow \ \frac{\boldsymbol{\tau}_{yy_{i,j}} - \boldsymbol{\tau}_{yy_{i,j-1}}}{\Delta y_{j-1/2}} \quad . \tag{4.29}$$

Finally, the convective term is treated in a way slightly different from T and $\boldsymbol{\tau}$:

$$\text{eq. for } u : \qquad (u.u_x)_{i-1/2,j} \rightarrow \begin{cases} u_{i-1/2,j}\dfrac{u_{i-1/2,j}-u_{i-3/2,j}}{\Delta x_{i-1}} & \text{if } u_{i-1/2,j} > 0 \\ u_{i-1/2,j}\dfrac{u_{i+1/2,j}-u_{i-1/2,j}}{\Delta x_i} & \text{if } u_{i-1/2,j} < 0 \end{cases} \tag{4.30}$$

$$(v.u_y)_{i-1/2,j} \rightarrow \begin{cases} \tilde{v}_{i-1/2,j}\dfrac{u_{i-1/2,j+1}-u_{i-1/2,j}}{\Delta y_{j+1/2}} & \text{if } \tilde{v}_{i-1/2,j} < 0 \\ \tilde{v}_{i-1/2,j}\dfrac{u_{i-1/2,j}-u_{i-1/2,j-1}}{\Delta y_{y-1/2}} & \text{if } \tilde{v}_{i-1/2,j} > 0 \end{cases} \tag{4.31}$$

$$\text{eq. for } v : \qquad (u.v_x)_{i,j-1/2} \rightarrow \begin{cases} \tilde{u}_{i,j-1/2}\dfrac{v_{i,j-1/2}-v_{i-1,j-1/2}}{\Delta x_{i-1/2}} & \text{if } \tilde{u}_{i-1/2,j} > 0 \\ \tilde{u}_{i,j-1/2}\dfrac{v_{i+1,j-1/2}-v_{i,j-1/2}}{\Delta x_{i+1/2}} & \text{if } \tilde{u}_{i-1/2,j} < 0 \end{cases} \tag{4.32}$$

$$(v.v_y)_{i,j-1/2} \rightarrow \begin{cases} v_{i,j-1/2}\dfrac{v_{i,j-1/2}-v_{i,j-3/2}}{\Delta y_{j-1}} & \text{if } v_{i,j-1/2} > 0 \\ v_{i,j-1/2}\dfrac{v_{i,j+1/2}-v_{i,j-1/2}}{\Delta y_y} & \text{if } v_{i,j-1/2} < 0 \end{cases} \tag{4.33}$$

where $\tilde{v}_{i-1/2,j}$ is the bilinear interpolation of v at the node of u and $\tilde{u}_{i,j-1/2}$ is the bilinear interpolation of u at the node of v.

4.3 Discretisation of the equations - adjoint system

• **Heat equation :**

$$-\ (U \cdot \nabla)\rho \ -\ \frac{1}{\text{Pe}}\Delta\rho \ +\ (\frac{1}{\text{We}})'(T)[1+\epsilon\frac{\text{We}}{\omega_r}\text{Tr}(\boldsymbol{\tau})]\boldsymbol{\tau} : \boldsymbol{\theta} = 0 \quad . \tag{4.34}$$

The discretisation of this equation is analogous to the one for the primal system. One only has to take care of the upwinding due to the sign "minus" in front of the convective term. The extra-term presents no difficulties :

$$(\boldsymbol{\tau} : \theta)_{i,j} \rightarrow (\ \boldsymbol{\tau}_{xx}\boldsymbol{\theta}_{xx} + \boldsymbol{\tau}_{yy}\boldsymbol{\theta}_{yy} + 2\tilde{\boldsymbol{\tau}}_{xy}\tilde{\boldsymbol{\theta}}_{xy}\ )_{i,j} \quad . \tag{4.35}$$

• **Stress equation :**

$$\text{We}(T)[-(U\cdot\nabla)\boldsymbol{\theta} - \boldsymbol{\theta}\cdot\nabla U - \nabla U^T\cdot\boldsymbol{\theta}\ ]\ +\boldsymbol{\theta}\ +\ \epsilon\frac{\text{We}}{\omega_r}[\text{Tr}(\boldsymbol{\tau})\boldsymbol{\theta} + (\boldsymbol{\tau}:\boldsymbol{\theta})\mathbf{I}] = -\text{We}(T)\mathbf{D}(\xi)\ . \tag{4.36}$$

This equation is very similar to the one for the primal stress. It is discretized following the same rules as before.

• **Momentum equation :**

$$\begin{aligned} &\text{Re}[\ -(U\cdot\nabla)\xi + \nabla U^T\cdot\xi\ ] - (1-\omega_r)\Delta\xi - \nabla\pi = \ -\mathcal{J}_U \\ &-2\frac{\omega_r}{\text{We}}\text{Div}\ \boldsymbol{\theta}\ -\ (\ \begin{array}{c}\partial_x\boldsymbol{\tau}:\boldsymbol{\theta}\\ \partial_y\boldsymbol{\tau}:\boldsymbol{\theta}\end{array}\ )\ -2\ \text{Div}\ (\boldsymbol{\theta}\ \boldsymbol{\tau})\ -\ \rho\ \nabla T \quad . \end{aligned} \tag{4.37}$$

This equation is more involved since it contains more terms than its primal counterpart. Nevertheless all terms can be discretized following the same rules as we already used for the primal equation.

4.4 Resolution of the primal system on one grid

The resolution method is based on the Gauss-Seidel iterative solver and a decoupling approach. We denote by Res_U ($Res_{\boldsymbol{\tau}}$,Res_T) the residual of the equation on velocity (stress, temperature). The flowchart of the algorithm is given on Figure 7. The basic tools for solving (P) and (D) are "Gauss-Seidel iterations" on velocity, stress and temperature. These are classical and not detailed. Here it suffices to mention that the number of iterations on the momentum, stress and heat equation, denoted by it_vel, it_temp and it_str, as well as the relaxation parameters used in the Gauss-Seidel solver, are of crucial importance. Concerning the order in which the equations of the system are treated, we solve first the equation on velocity, then the one on temperature, and eventually the stress equation. This order seems to be natural, since the temperature does not depend on the stress and whereas the stress is strongly dependant on the temperature. Moreover, we start with the equation on velocity since it is meaningless to solve the heat and stress equations without a velocity field. Note that if we take large it_vel, it_temp and it_str, the method is "fully" decoupled, while small numbers of iterations lead to a coupling between the equations.

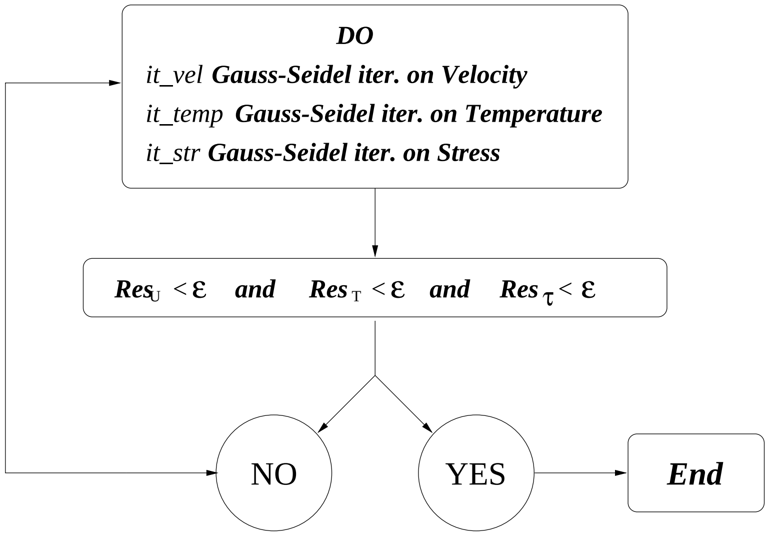

Fig 7: Algorithm on one grid

4.5 Multigrid algorithm

The multigrid algorithm which we employ is a modification of the algorithm "FAS" introduced by A.Brandt [3]. The modification consists in simplifying the flowchart of "FAS" by prescribing in advance the number of iterations that will occur in the fine, intermediate and coarse grids. The residuals on the equations are also only checked on the fine grid. The advantage of this simplification is given in [15]. This algorithm has been used by C.Jouron [15] for the resolution of the Navier-Stokes equations, and by Al.Moatassime [20] and Marduel [19] for the resolution of isothermal viscoelastic flows. The flowchart for a "V-Cycle" is given in Figure 8.
We fix a family of grids $(\Omega_r), r = 1, ..., n$, with Ω_n being the finest. The goal is to solve (P) on the finest grid. This is expressed as :

$$L_n(U_n, p_n, \boldsymbol{\tau}_n, T_n) = 0 \quad . \tag{4.38}$$

Thus L_n is a non-linear operator of finite dimension. We define a restriction operator $\mathcal{R}_r^{r-1}$ from grid Ω_r to grid Ω_{r-1}, which maps a vector $(U, p, \boldsymbol{\tau}, T)$ defined on Ω_r to its interpolated defined on grid Ω_{r-1} . We also define a prolongation operator $\mathcal{P}_r^{r+1}$ from grid Ω_r to the grid Ω_{r+1}, which maps a vector defined on grid Ω_r to its extension on the grid Ω_{r+1}. The operator $\mathcal{M}_r^{it}$ on $(U, p, \boldsymbol{\tau}, T)$ is the one that performs on the grid Ω_r first it_vel Gauss-Seidel iterations on the velocity and pressure, then it_temp Gauss-Seidel iterations on temperature, and finally it_str Gauss-Seidel iterations on stress, and all of this it times. Finally, we introduce the right hand side b_k defined on all the grids, with a zero value on the finest grid $(k = n)$, but non zero values on the coarser grids as indicated more precisely in the multigrid algorithm given by :

- $(U_0, p_0, \boldsymbol{\tau}_0, T_0)$ initial approximation of the solution of (P).

Smoothing on the finest grid

- $k \leftarrow n$

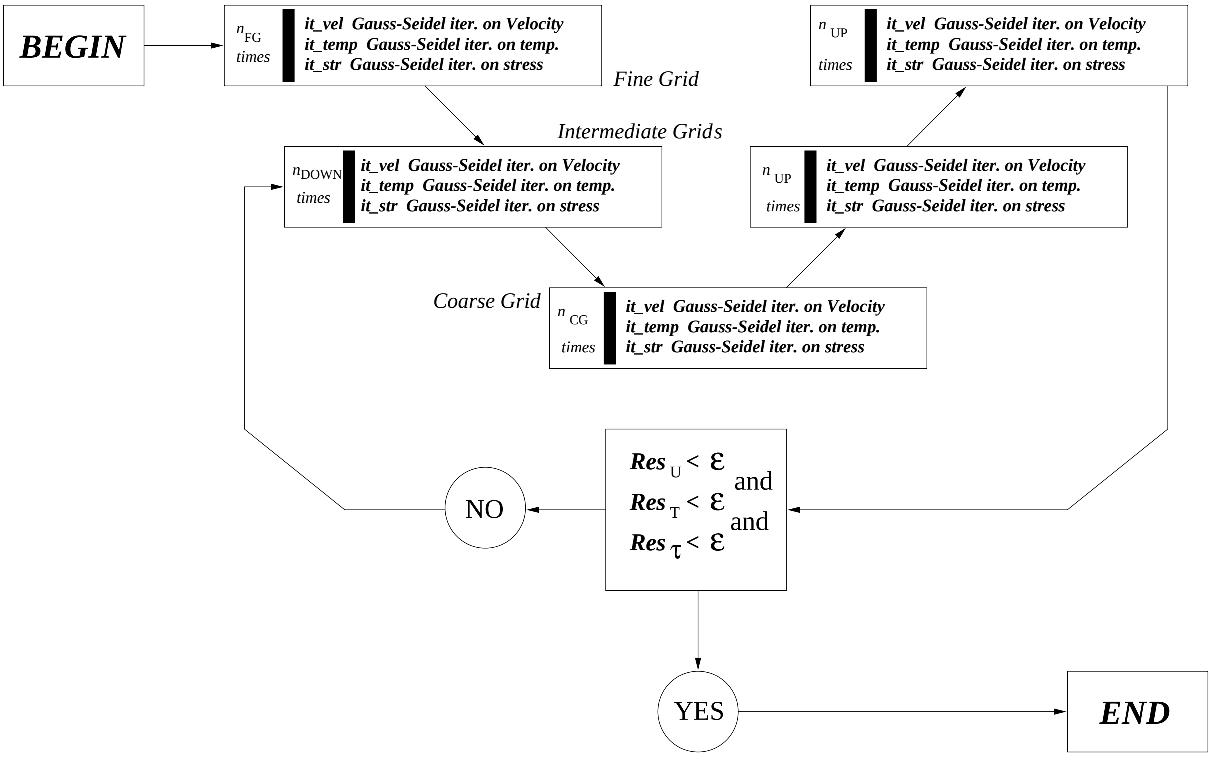

Fig 8: Multigrid Algorithm

• $b_n = 0$
• $(U_n, p_n, \boldsymbol{\tau}_n, T_n) = \mathcal{M}_n^{m_n}(U_n, p_n, \boldsymbol{\tau}_n, T_n)$ $\;\; m_n$ iterations on grid Ω_n .

Descent stage

• $k \leftarrow k-1$
• $b_k = \mathcal{R}_{k+1}^k(b_{k+1} - L_{k+1}(U_{k+1}, p_{k+1}, \boldsymbol{\tau}_{k+1}, T_{k+1})) + L_k(\mathcal{R}_{k+1}^k(U_{k+1}, p_{k+1}, \boldsymbol{\tau}_{k+1}, T_{k+1}))$
calculus of the new right hand side on grid Ω_k
• $(U_k, p_k, \boldsymbol{\tau}_k, T_k) = \mathcal{M}_k^{m_k}(U_k, p_k, \boldsymbol{\tau}_k, T_k)$ $\;\; m_k$ iterations on grid Ω_k .

• If $k > 1$ go to the descent stage
Else go to the ascent stage

Ascent stage

• $k \leftarrow k+1$
• $(U_k, p_k, \boldsymbol{\tau}_k, T_k) = (U_k, p_k, \boldsymbol{\tau}_k, T_k) + \mathcal{P}_{k-1}^k((U_{k-1}, p_{k-1}, \boldsymbol{\tau}_{k-1}, T_{k-1}) - \mathcal{R}_k^{k-1}(U_k, p_k, \boldsymbol{\tau}_k, T_k))$
correction of the solution on grid Ω_k
• $(U_k, p_k, \boldsymbol{\tau}_k, T_k) = \mathcal{M}_k^{m_k}(U_k, p_k, \boldsymbol{\tau}_k, T_k)$ $\;\; m_k$ iterations on grid Ω_k .

• If $k < n$ go to the ascent stage
Else go to the stage "Convergence Test on the finest grid"

Convergence test on the finest grid

- Convergence not reached : go to the descent stage
- Convergence reached : END OF THE ALGORITHM

4.6 Resolution of the adjoint system

To solve the adjoint system we use the same multigrid algorithm as for the primal system, excepted that we solve *first* the momentum equation, *then* the stress equation and *finally* the heat equation. Indeed in this case the dual stress equation does not depend on the dual temperature, and the dual temperature does depend on the dual stress. Let us point at some additional differences. It has to be noted that due to the sign "minus" in front of the convective terms $(U \cdot \nabla)\xi$, $(U \cdot \nabla)\boldsymbol{\theta}$ and $(U \cdot \nabla)\rho$, the outflow for the primal system plays the role of the inflow for the dual system. Thus we shall impose a "reversed" enumeration of the unknowns, that is, the Gauss-Seidel iterations are performed from the right to the left. This is an obviously necessity for the dual stress equation. It is not so necessary for the dual momentum equation, the size of the Reynolds number being so small that it has no essential influence on the speed of the resolution. For the dual heat equation, the fact that the transport occurs from the right to the left and that the boundary conditions at the "dual inflow" are of Robin type causes extra difficulties. Indeed, one cannot begin an iteration of Gauss-Seidel from the right since the values of ρ on this boundary are unknown. To circumvent this difficulty, we will first perform one Gauss-Seidel iteration from the left to the right (where the boundary conditions at the "dual outflow" are : $\rho = 0$), and then one Gauss-Seidel iteration from the right to the left. The first iteration from the left to the right gives us a value noted ρ_{try} at the "dual inflow". Thus for the iteration from the right to the left, we use the following boundary condition :

$$\frac{1}{\mathrm{Pe}} \partial_n \rho = -u \rho_{try} \quad . \tag{4.39}$$

The efficiency of this procedure was checked successfully on one dimensional advection-diffusion problems before it was utilized to solve the adjoint system. The Gauss-Seidel iteration for the variable corresponding to temperature of the dual system is given in detail in Appendix **B**.

4.7 Resolution of the control problem : coupling between the primal system and the adjoint system

To minimize the cost functional, we utilize a gradient algorithm . The simplest gradient algorithm is written as :

1. Set $k = 0$ and choose $\mathbf{g}^0$
2. Evaluate $\nabla \mathcal{J}(\mathbf{g}^k)$
3. Choose an descent step $h > 0$
4. Set $\mathbf{g}^{k+1} = \mathbf{g}^k - h\, \nabla \mathcal{J}(\mathbf{g}^k)$.

5. Set $k \leftarrow k+1$, and goto 2

The gradient $\nabla\mathcal{J}(\mathbf{g}^k)$ can be expressed as :

$$\nabla\mathcal{J}(\mathbf{g}^k) = \frac{1}{\mathrm{Pe}}\partial_n\rho + \gamma.\mathbf{g}^k \qquad \text{on } \Gamma_c \quad , \tag{4.40}$$

where $\rho = \rho(\mathbf{g}^k)$. The derivation of (4.40) is given in Appendix **A**. Note that the evaluation of $\nabla\mathcal{J}(\mathbf{g}^k)$ requires the solution of (P) and (D). As for any gradient algorithm, the step length h must be chosen adequately. The optimization problem $(\mathcal{P})$ is too complicated to propose a sophisticated line search. Rather we proceed by interpolation-extrapolation. Given $\mathbf{g}^k$, the descent direction $\nabla\mathcal{J}(\mathbf{g}^k)$ and the cost at iteration k, denoted by $\mathcal{J}^0$, we choose two steps lengths h_1 and h_2 and calculate the corresponding new controls $\mathbf{g}_1^{k+1}$ and $\mathbf{g}_2^{k+1}$ (step 4 of the algorithm) and corresponding costs $\mathcal{J}^1$ and $\mathcal{J}^2$. Then $\mathcal{J}$ is interpolated quadratically between $\mathcal{J}^0$, $\mathcal{J}^1$ and $\mathcal{J}^2$, and approximating optimal step length h_{app} by which the algorithm is advanced is chosen as the minimizer of the quadrature interpolation. The conjugate gradient algorithm, that we finally utilize, doesn't require more work than the previous gradient algorithm. The algorithm is :

1. Set $k = 0$ and choose $\mathbf{g}^0$
2. (a) Evaluate $\nabla\mathcal{J}(\mathbf{g}^k)$
   (b) If $k = 0$ then $\mathcal{D}^k = \nabla\mathcal{J}(\mathbf{g}^k)$
   else $\mathcal{D}^k = \nabla\mathcal{J}(\mathbf{g}^k) + \beta_k\ \mathcal{D}^{k-1}$
3. Choose an descent step $h > 0$
4. Set $\mathbf{g}^{k+1} = \mathbf{g}^k - h\ \mathcal{D}^k$.
5. Set $k \leftarrow k+1$, and goto 2

The descent direction to update the control is no more the gradient direction. The coefficient β_k in given by the *("Polak-Ribiere")* relation :

$$\beta_k = \frac{(\ \nabla\mathcal{J}(\mathbf{g}^k)\ ,\ \nabla\mathcal{J}(\mathbf{g}^k) - \nabla\mathcal{J}(\mathbf{g}^{k-1})\ )}{||\nabla\mathcal{J}(\mathbf{g}^{k-1})||^2_{\mathrm{L}^2(\Gamma_c)}} \tag{4.41}$$

In practice, we always start from $\mathbf{g}^0 = 0$, and the two first descent steps are $h_1 = 20$ and $h_2 = 10$. Then for the next iterations, we use for h_1 the value h_{app} of the previous iteration, and $h_2 = h_1/2$. We find that the conjugate gradient algorithm behaves only a little better than the gradient algorithm for our problem.

5 Numerical results and discussion

5.1 Meshes

For isothermal viscoelastic fluid flow, we previously used the mesh M1 (Figure 9 left) in [19]. However, for the present work a higher precision of the vortex intensity in the recirculation zone is necessary. In addition a fine resolution of the temperature which governs the control mechanism in the recirculation zone is required. For these reasons we used a refined mesh M2, twice finer than M1. The main characteristics of these two meshes are given in Table

1. Note that the mesh is also refined near the wall of the upstream channel in order to evaluate properly the optimality condition given by

$$\text{(OC)} \qquad \gamma.\mathbf{g} = -\frac{1}{\mathrm{Pe}}\partial_n \rho \quad \text{on } \Gamma_c \quad . \tag{5.1}$$

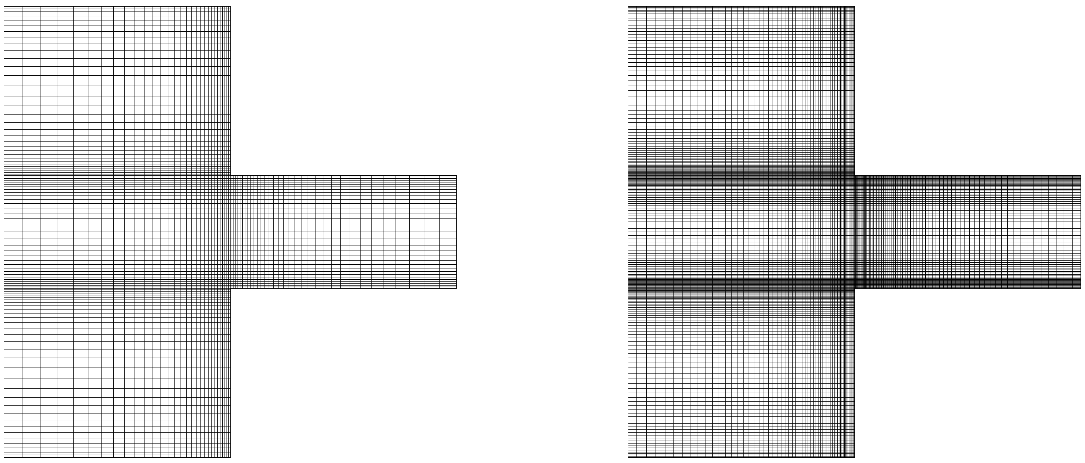

Fig 9: Meshes M1 (left) and M2 (right) near the contraction zone

TABLE 1: Characteristics of meshes M1-M2

No. of / Mesh	M1	Smallest cell	M2	Smallest cell
Cells	7680	0.03 $\times$0.025	30720	0.015 $\times$0.0125
Unknowns	53712		214848	

5.2 Choice of the parameters.

The numerical simulations were performed with the following parameters : $\mathrm{Re} = 10^{-5}$, $\mathrm{Pe} = 100$, $\omega_r = 0.89$, $\mathrm{We} = 10$, $\epsilon = 0.2$. Indeed, for this kind of flow, the Prandtl number for viscoelastic fluid is in the order of magnitude of $\mathrm{Pr} = 10^8$ (see [22]). Since we have

$$\mathrm{Pr} = \frac{\mathrm{Pe}}{\mathrm{Re}} \quad , \tag{5.2}$$

the value of Pr is consistent with our choice for Re and Pe. The flow rate is set to $\frac{2}{3}$, which implies that the shear rate at the wall of the downstream channel is about 1. We have also truncated the function f of the WLF model (Figure 10) : indeed, as we shall see, the control mechanism will require a significant amount of cooling. In extreme cases this can lead to the so-called "High Weissenberg Number Problem". Thus, as shown in Figure 10, we set

$$f_{tr}(T) = \begin{cases} \exp(-\dfrac{c_1 \cdot T}{c_2 + T}) & \text{if } T > T_{tr} \quad ; \\ \\ f(T_{tr}) & \text{otherwise.} \end{cases} \tag{5.3}$$

to avoid this problem. We have chosen $T_{tr} = -4$, such that in the region where the temperature is highly negative the Weissenberg number can reach a maximum that is at most 3.8 times higher than our reference Weissenberg number.

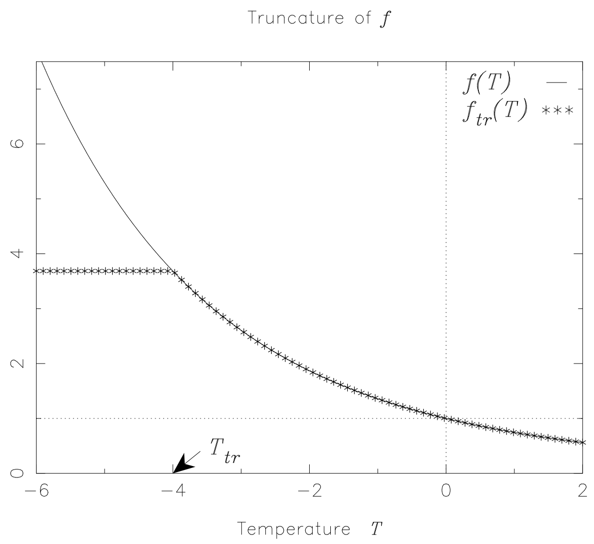

Fig 10: Truncation of the function f

5.3 Domain of observation and domain of control

We choose our domain of observation $\tilde{\Omega}_i$ ($i = 1, 2$ for the two cost functionals $\mathcal{J}_1$ and $\mathcal{J}_2$) and domain of control Γ_c as shown in Figure 2. More precisely, we have

$$\tilde{\Omega}_1 = [-04.0 : -0.10] \times [-3.99 : -2.50] \ \cup \ [-04.0 : -0.10] \times [+2.50; +3.99] \tag{5.4}$$

$$\tilde{\Omega}_2 = [-04.0 : -0.01] \times [-3.99 : +3.99] \tag{5.5}$$

These are roughly the regions where most of the recirculation which should be reduced by means of thermal control takes place. Concerning Γ_c, numerical experiments have shown us that the whole boundary near the corners (vertical and horizontal walls) has to be taken into account. Obviously, heating or cooling the boundaries after the re-entrant corners have no effect on the upstream flow. Thus :

$$\Gamma_c = [-15.0 : 0.0] \ \text{ on horizontal walls, upstream channel} \tag{5.6}$$

$$\Gamma_c = [-4.0 : -1.5] \cup [+1.5 : +4.0] \ \text{ on vertical walls, upstream channel} \tag{5.7}$$

5.4 Parameters of the cost functionals

The choice of the parameters α and γ is of crucial importance. More precisely, we have taken a large value for α so that the "body force" due to the derivative $\mathcal{J}_U$ in the adjoint momentum equation is strong. Indeed, considering the optimality condition, we note that -if we want to have a chance to control the flow- the dual temperature must be sufficiently large. The source term in the adjoint heat equation being

$$(\frac{1}{\mathrm{We}})'(T)[1+\epsilon\frac{\mathrm{We}}{\omega_r}\mathrm{Tr}(\boldsymbol{\tau})]\boldsymbol{\tau}:\boldsymbol{\theta} \quad , \tag{5.8}$$

with $\boldsymbol{\tau}$ small in the corners, we need large $\boldsymbol{\theta}$ so that this source term is not too small. This is achieved by a strong stream function for the dual velocity and explains our choice of a large α value. Finally, we have chosen $\alpha = 1000$ for $\mathcal{J}_1$. Then, in order to achieve a well balanced cost for the control and the state, we have chosen $\gamma = 0.0005$. For $\mathcal{J}_2$, we have set $\alpha = 200000$ and $\gamma = 0.0001$.

Applying the conjugate gradient algorithm for the resolution of our problem, we show in Figure 11 the decrease of the costs functions $\mathcal{J}_1$ and $\mathcal{J}_2$ as a function of the iterations of the algorithm. For both cost functionals we observe a significant reduction of the total

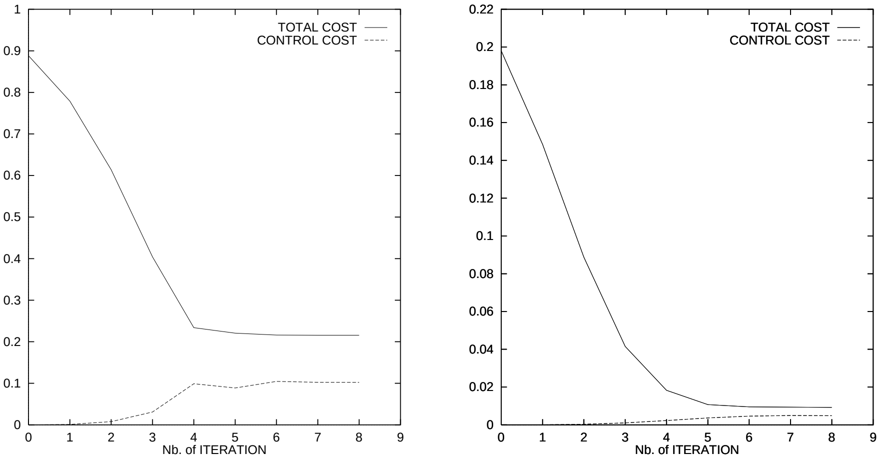

Fig 11: Cost decrease for $\mathcal{J}_1$ (left) and $\mathcal{J}_2$ (right)

cost during the course of the iterations.

5.5 Final control g and temperature distribution

The controls that we obtain for $\mathcal{J}_1$ and $\mathcal{J}_2$ are quit different. We first note that in both cases we have to cool a lot near the re-entrant corners. But the amount of cooling differs significantly between $\mathcal{J}_1$ and $\mathcal{J}_2$ (Figure **??**). On the horizontal walls (HW) of the upstream channel, we obtain a mainly positive temperature in the case of $\mathcal{J}_1$, with a maximal temperature of $T_{max} \simeq 4.0$, while $T_{max} \simeq 1.0$ in the case of $\mathcal{J}_2$, with a portion of (HW) with negative temperature near the corners. The distribution of the temperature in the whole domain is also given (Figure 13).

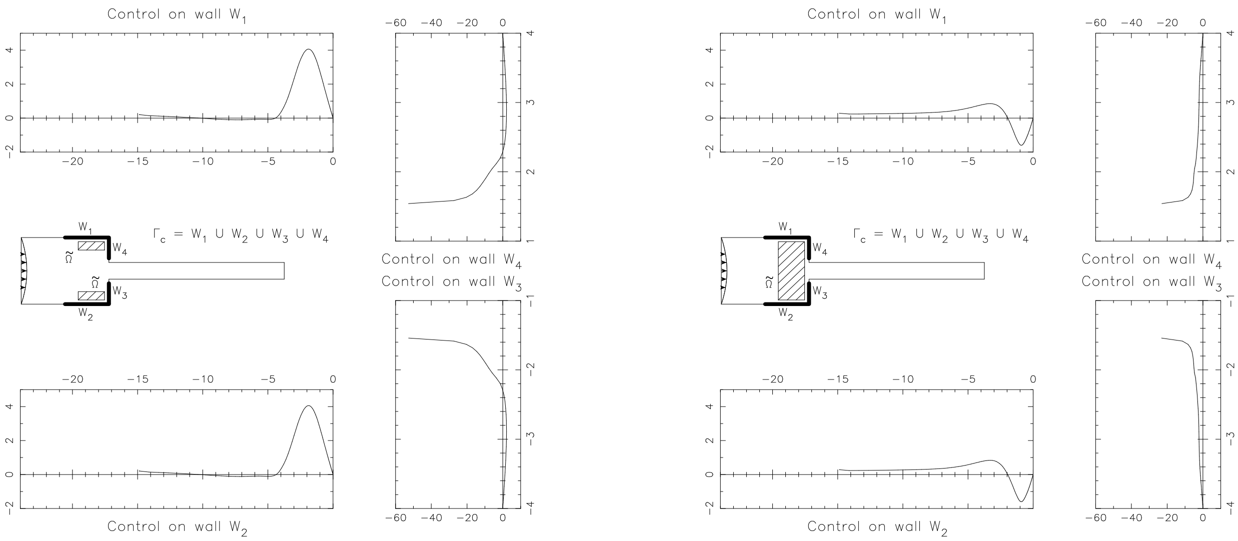

Fig 12: Control $\mathbf{g}$ on the boundaries for $\mathcal{J}_1$ (left) and $\mathcal{J}_2$ (right)

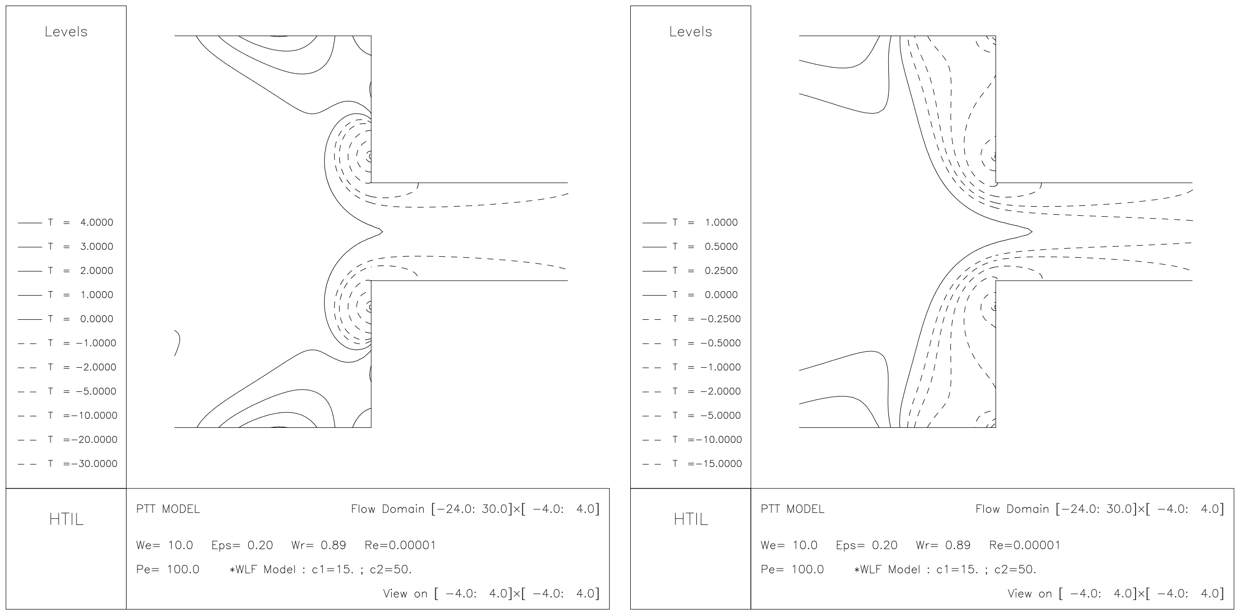

Fig 13: Temperature distribution for $\mathcal{J}_1$ (left) and $\mathcal{J}_2$ (right)

5.6 Stream functions of the controlled-uncontrolled flows

We first give the flow's streamlines of an uncontrolled viscoelastic fluid, and the ones of a viscous fluid (Figure 14). This latter is the flow we will use for our reference velocity field in $\mathcal{J}_1$.
The streamlines of the controlled flows according to the two cost functionals are given in Figure 15. We have used in Figures 14 and 15 the same levels for plotting the stream function, with values 1 and -1 on the upper and lower boundary. We note that the recirculation zone for $\mathcal{J}_1$ is drastically reduced. The reduction is less strong for $\mathcal{J}_2$. Remembering the shapes of the controls for these two cost functionals, we can affirm : cooling the vertical walls (VW) leads to a reduction in the recirculation zone and the intensity of the vortex. But it is the combination of cooling on (VW) and heating on (HW) that produces a dramatic reduction of the recirculation zone (Figure 15 left). We performed also simulations with heating on (HW), on (VW) or on both : this action has no effect on the recirculation zone.
The maximal intensity of the vortex for the uncontrolled flow is $FC_{max} = 1.0034$. We obtain $FC_{max} = 1.0003$ considering the controlled flow with $\mathcal{J}_1$ and $FC_{max} = 1.0007$ for $\mathcal{J}_2$. We give in Figure 16 a zoom on these vortices. This maximal intensity occurs for $\mathcal{J}_1$ in the "lip vortex", and the vortex intensity in the corners is $FC_{max} = 1.00005$ (Figure 16).
The goal of reducing the recirculation zone was achieved with both cost functionals. The numerical results shows that a good cost decrease for a given cost functional ($\mathcal{J}_2$) does not imply that the goal will be better reached. We obtain better results with $\mathcal{J}_1$, although the cost is divided by a factor 4, compared to a factor 20 for $\mathcal{J}_2$ (see Figure 11).

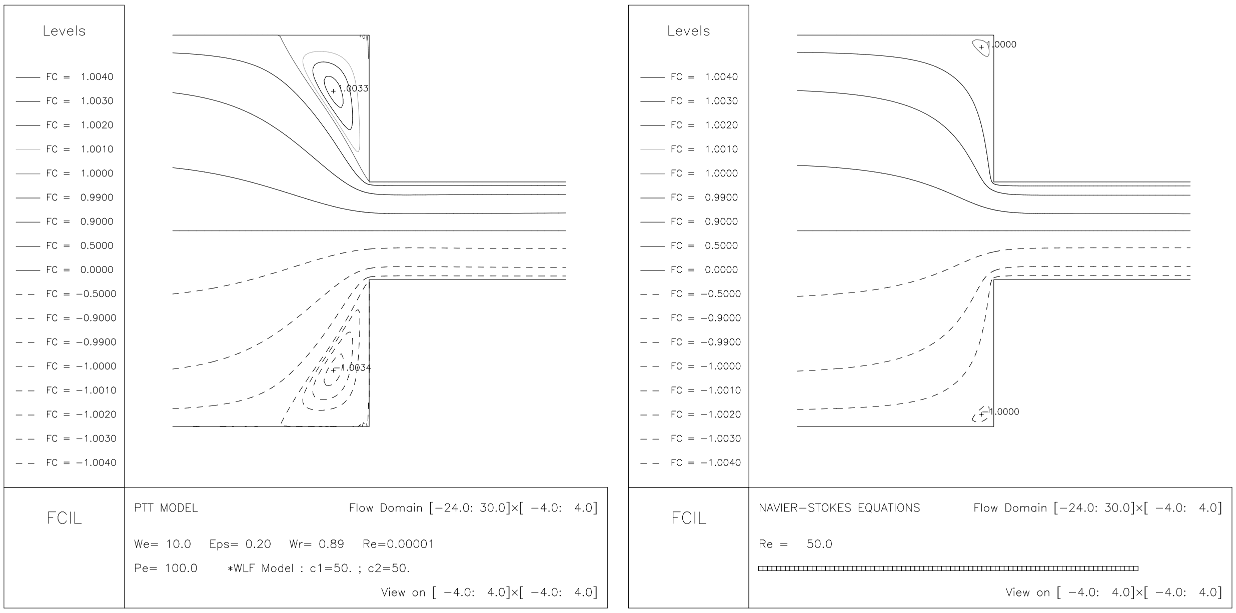

Fig 14: The two streamfunctions for a viscoelastic fluid with no temperature (left) and for a viscous fluid (right)

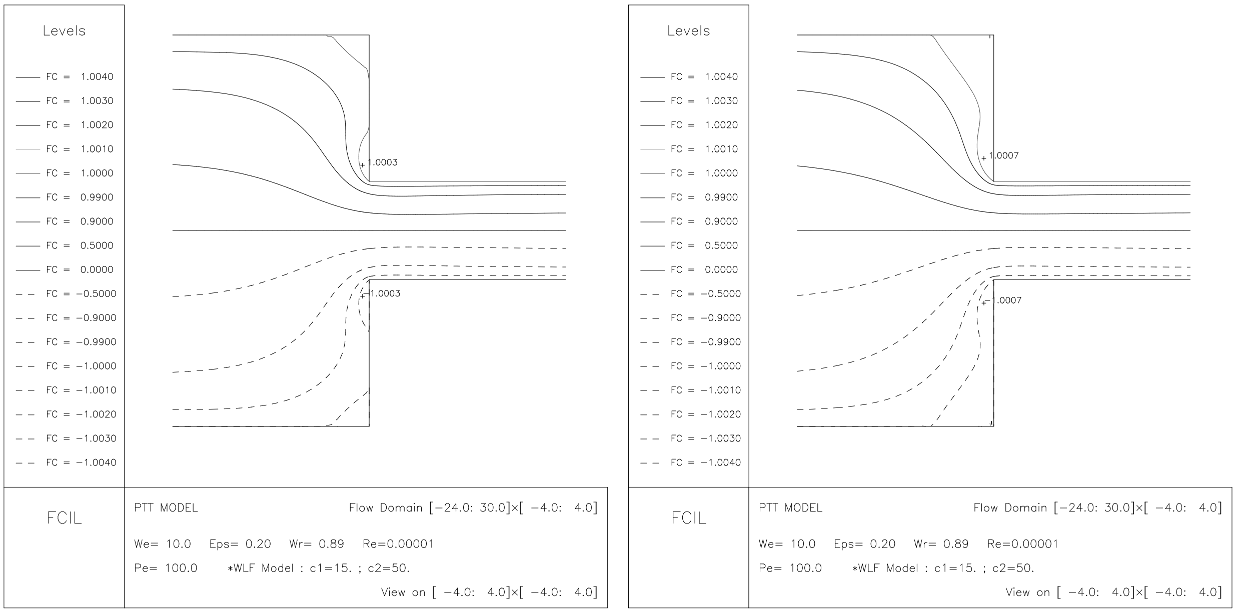

Fig 15: The two streamfunctions of the controlled flows for $\mathcal{J}_1$ (left) and $\mathcal{J}_2$ (right)

5.7 Stress of the controlled and uncontrolled flows

We compare the stress for the uncontrolled and controlled flow with cost functional $\mathcal{J}_1$. Figures 17 to 22 give the three components of the stress for these two flows. The stress does not reach high values at the re-entrant corner, due to our choice of the parameter $\epsilon = 0.2$, which is rather large. Nevertheless, we note a strong difference for the component τ_{xy} of the stress in the recirculation zone. Component τ_{yy} is also slightly different, while no apparent differences are visible for τ_{xx}.

5.8 Dual variables

The dual variables have no physical signifiance. We give here the streamfunction and curl of the dual velocity, dual stress and temperature just for information (Figures 25 to 26). We note that, due to the high values of α in the cost functionals, the dual velocity reaches high values, as for the dual stress, but the dual temperature is one order of magnitude inferior to the dual stress.

5.9 A few more experiments

In this section we check numerically our hypothesis concerning the (non)influence of a constant solvent viscosity (section 2.4) on our calculations. With given temperature boundary conditions, we solve the primal system (P) twice : a first time with a constant solvent viscosity (case -a-), then with a temperature dependant solvent viscosity (case -b-), where the solvent viscosity follows the same temperature dependancy as η_V and We :

$$\eta_S(T) = (1 - \omega_r).f(T) \tag{5.9}$$

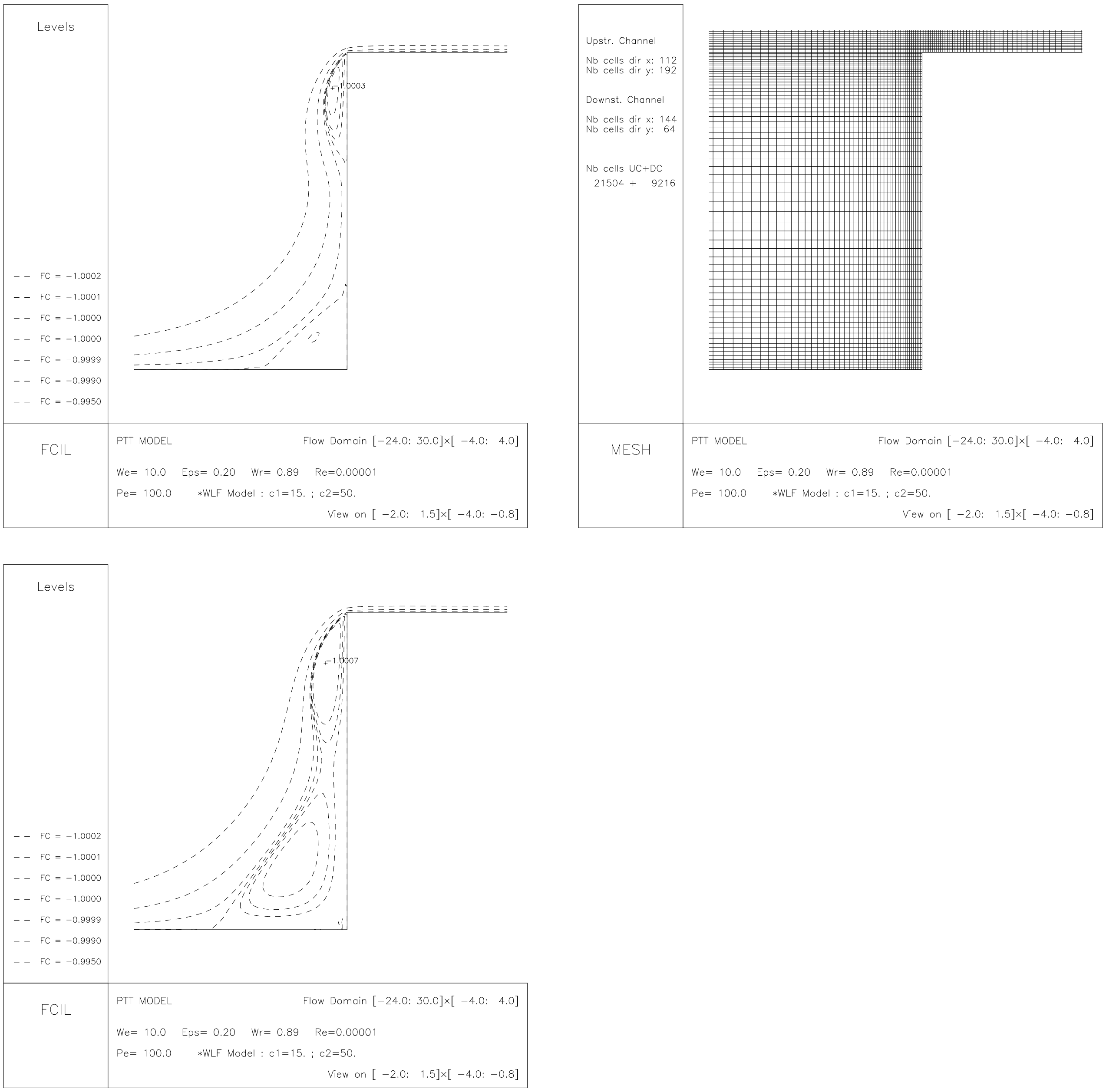

Fig 16: Streamfunctions for $\mathcal{J}_1$ (high), $\mathcal{J}_2$ (low) and zoom on the mesh

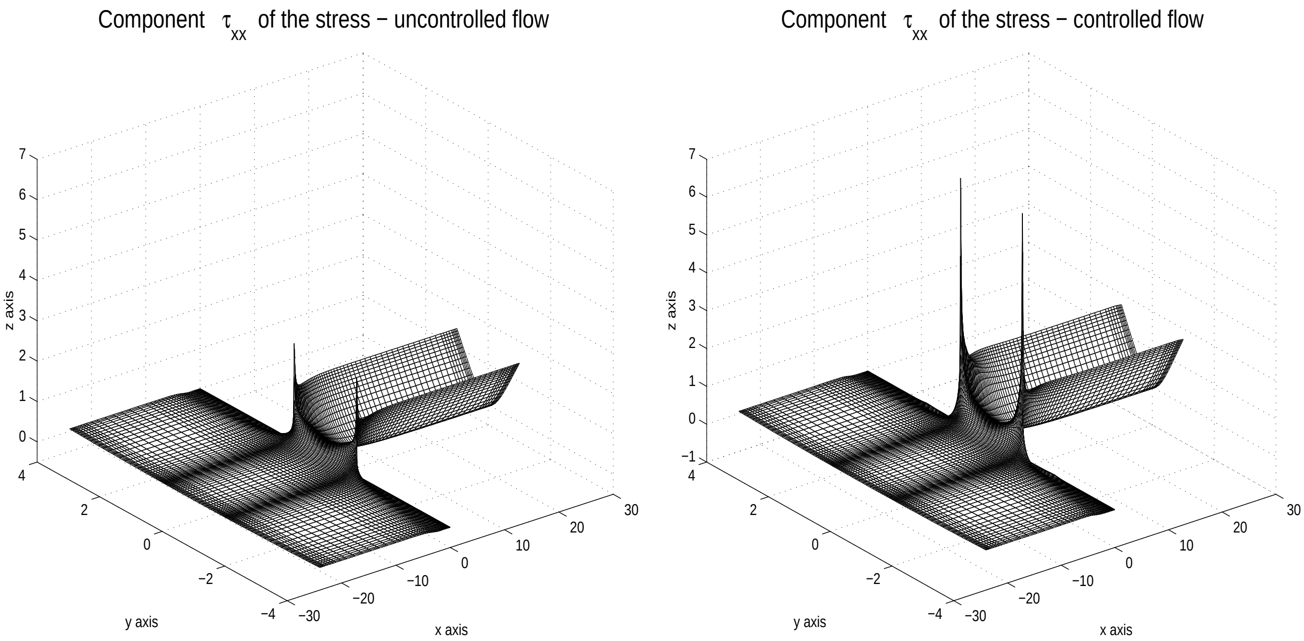

Fig 17: Component τ_{xx} of the stress for the uncontrolled and controlled flows

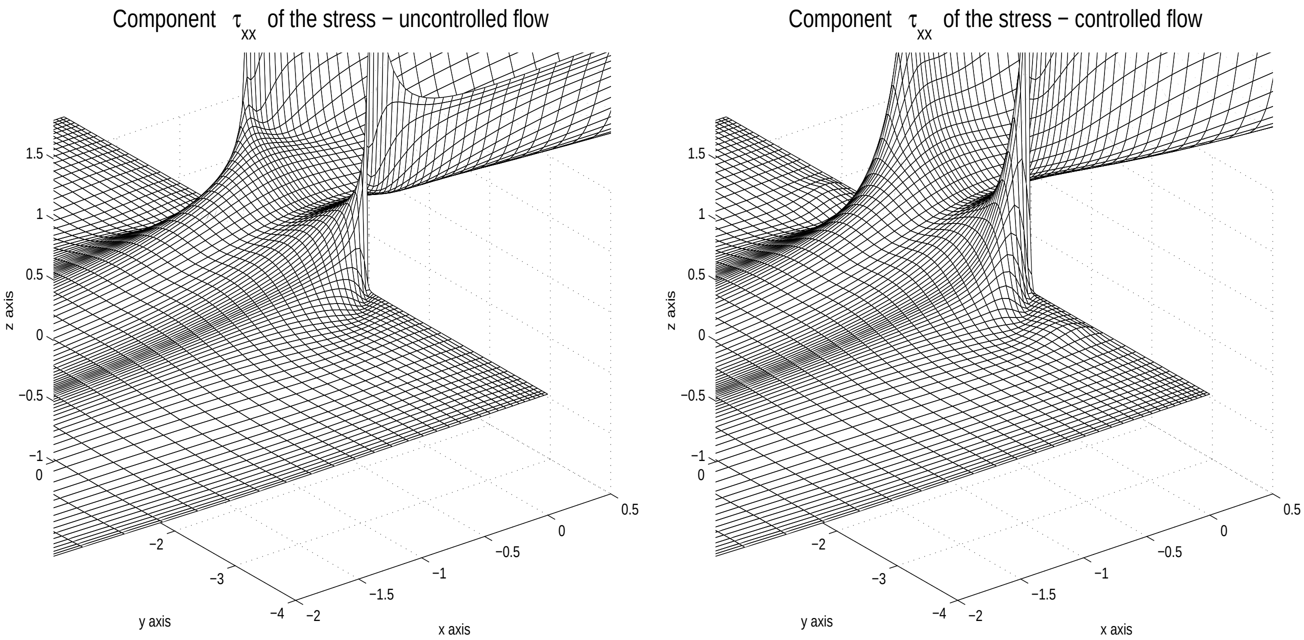

Fig 18: Component τ_{xx} of the stress for the uncontrolled and controlled flows - zoom

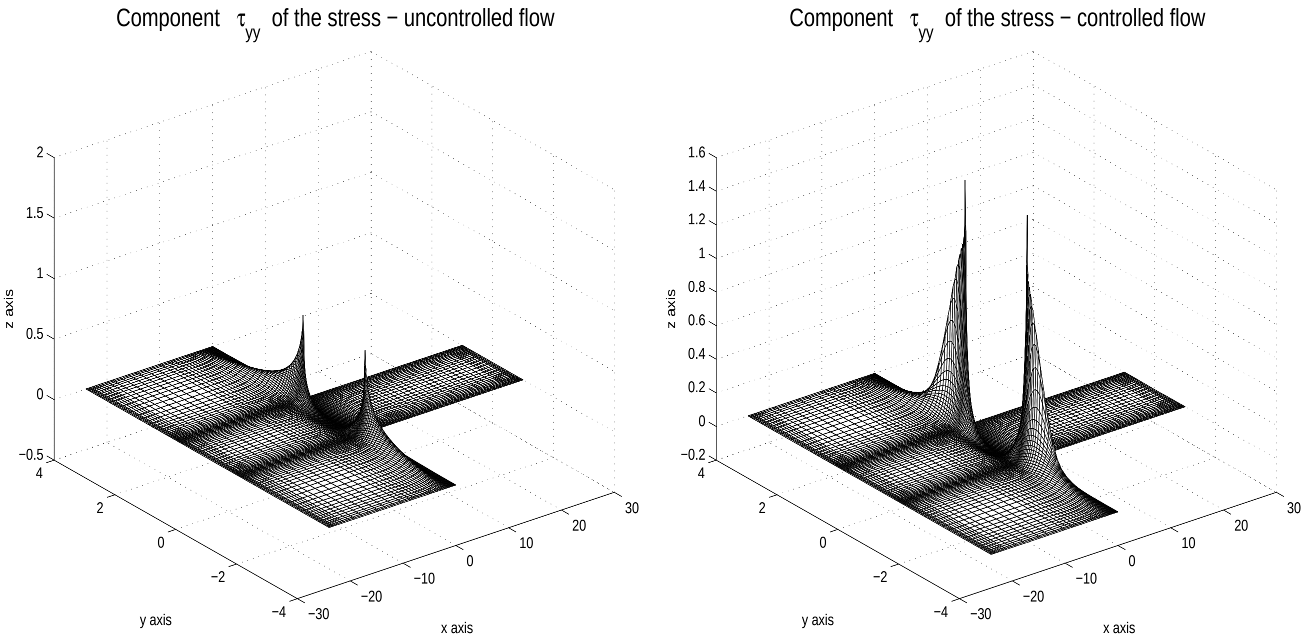

Fig 19: Component τ_{yy} of the stress for the uncontrolled and controlled flows

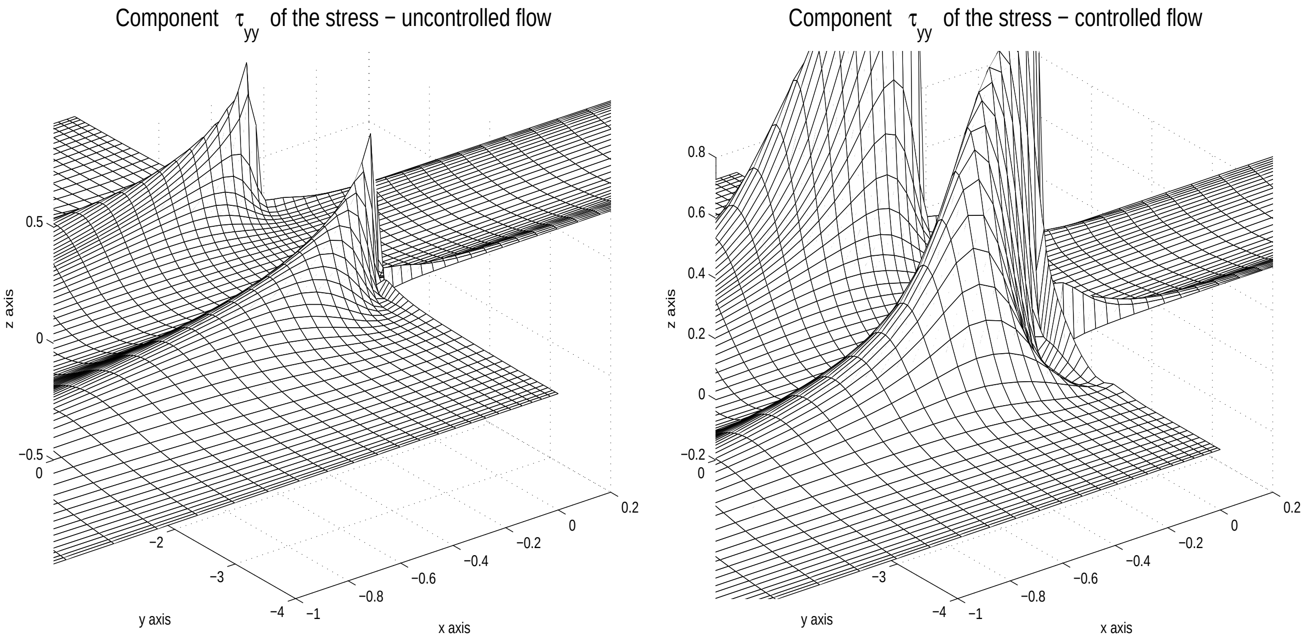

Fig 20: Component τ_{yy} of the stress for the uncontrolled and controlled flows - zoom

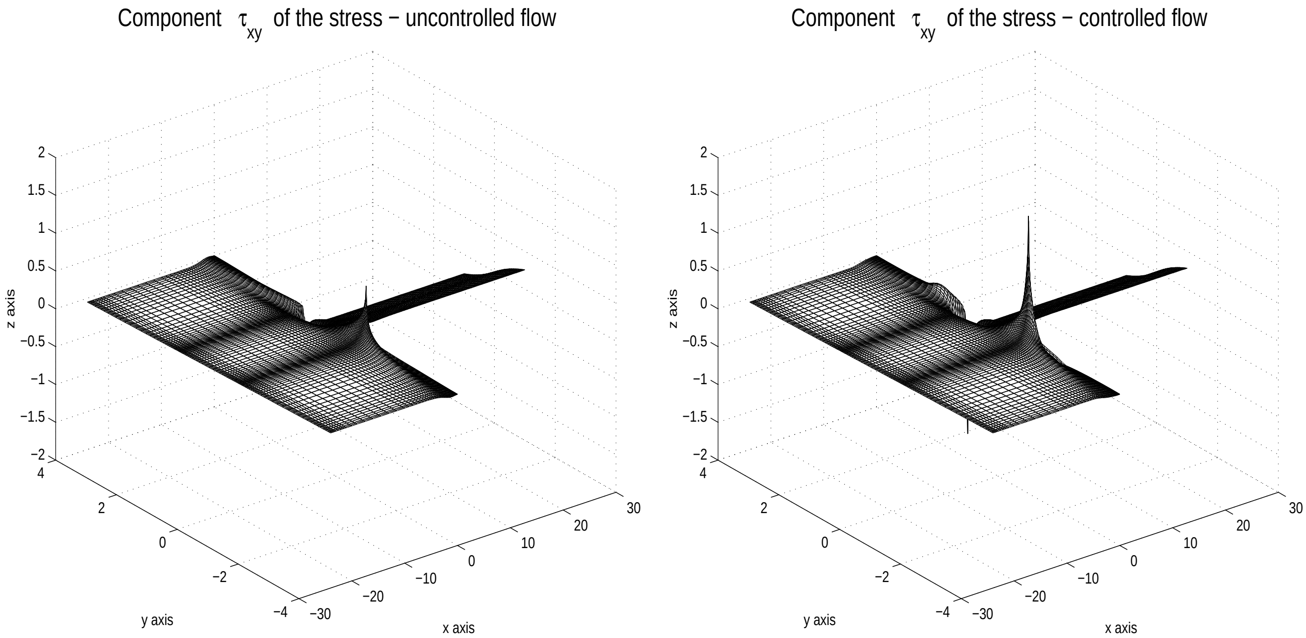

Fig 21: Component τ_{xy} of the stress for the uncontrolled and controlled flows

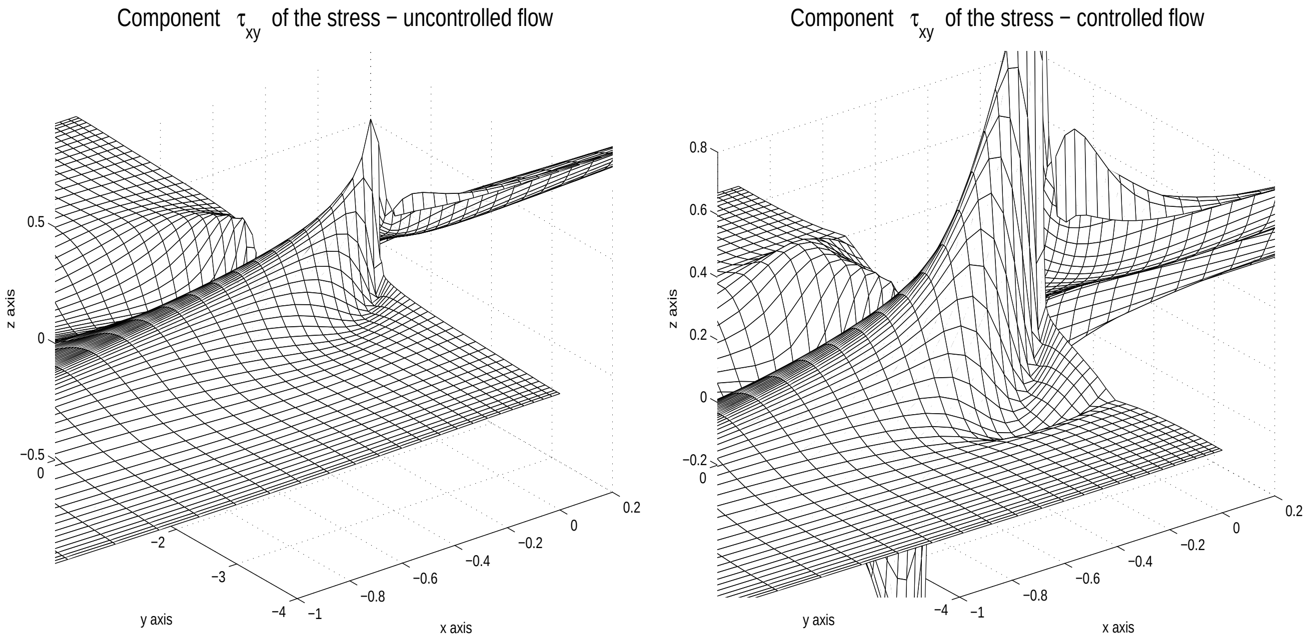

Fig 22: Component τ_{xy} of the stress for the uncontrolled and controlled flows - zoom

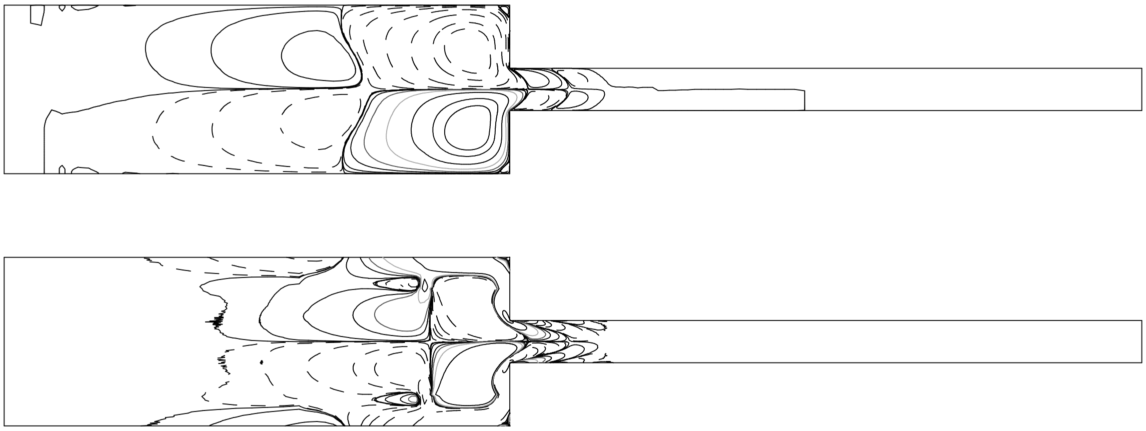

Fig 23: Streamfunction (upp) and curl (bottom) of the dual velocity in the domain

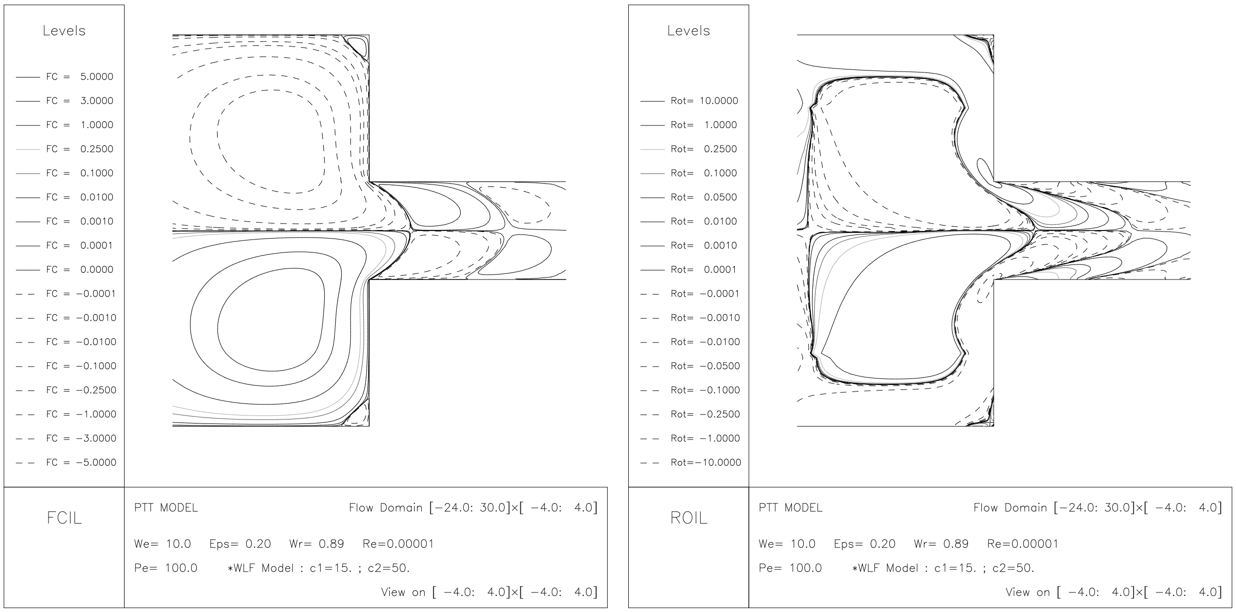

Fig 24: Streamfunction (left) and curl (right) of the dual velocity : zoom

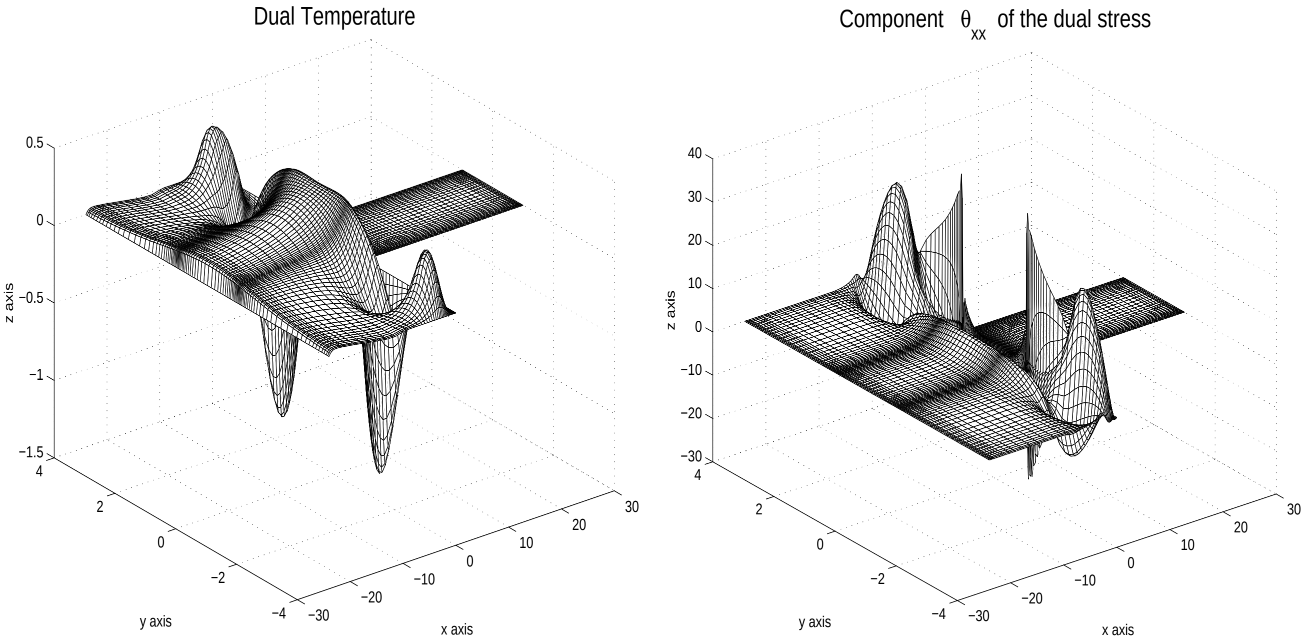

Fig 25: Dual temperature and dual stress θ_{xx}

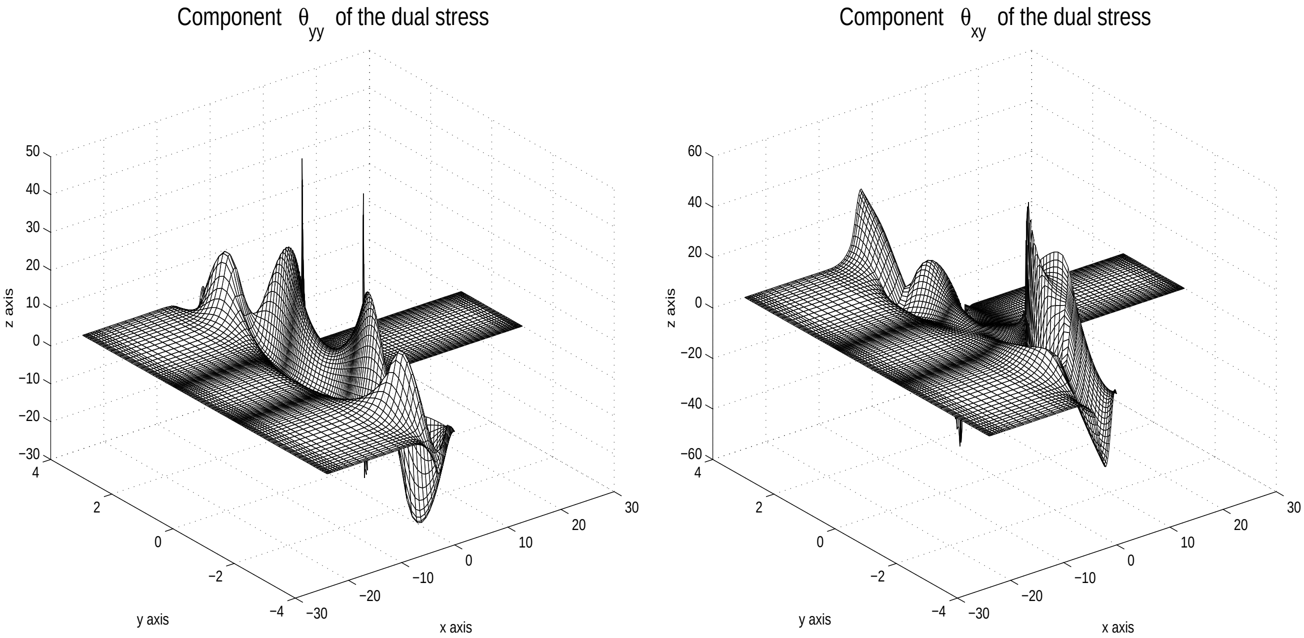

Fig 26: Dual stress θ_{yy} and θ_{xy}

where f is given by 5.3.

We also compare the results obtained in cases -a- and -b- with two differents temperature boundary conditions. First we impose on Γ_c a control shown in Fig 27 : a positive temperature on W_2, and a negative one on W_3, while on W_1 and W_4 no temperature is imposed (Neumann conditions for the heat equation on this part of the boundary). The resulting flows for cases -a- and -b- are given on Fig 27.

Next, we impose on both W_2 and W_3 a strong heating, while no control is set on W_1 and W_4, as depicted on Fig 28. The resulting flows for cases -a- and -b- are given on Fig 28.

For these two controls, there are no major differences between case -a- and case -b-. Our first test shows that it is not neccesarry to impose a very strong cooling on W_3 (as founded by our calculations, see Fig 12) to obtain a significant reduction of the vortex. The results of the second test (strong heating on all boundary) show that this control doesn't lead to a diminution of the vortex, but to the inverse. Obviously, the vortex size would be reduced, if with η_S and η_V constants, *only* the Weissenberg number would depend on the temperature : then the "elastic part" of the fluid would diminush as the temperature growthes. But with *both* Weissenberg number *and* elastic viscosity depending on the temperature. As temperature increases, we cannot say the elastic part of the fluid decreases.

We did not find similar simulations in the literature, nor physical experiments to confirm our simulations. Nethertheless, in the case of isothermal simulations, the results we obtain in term of vortex size and intensity are similar to the many ones depicted for the 4 to 1 contaction flow.

5

6 Conclusions

The main goal of this research was to investigate the feasibility of thermal control of a viscoelastic fluid by boundary control on a portion of its boundary. For this purpose the PTT model was extended to a "non-isothermal" PTT model. (Though many non-isothermal models had been already used in the literature, this one was chosen for its simplicity). Optimal control problems are formulated with the aim to influence and more precisely to reduce the large recirculation zones typical for viscoelastic fluids at the corners of the reduction of the channel. A first order necessary optimality system is derived by means or a Lagrangian formalism resulting in a system consisting of the primal equations, the dual equations and the optimality condition.

Once the optimality system is obtained it is simple to also find a formula for the gradient of the cost functional with respect to the control variable. The gradient is the essential tool to start an iterative minimization process. It requires to solve the primal and the dual system at every stage of the iteration. Numerically this was achieve by means of a finite difference scheme set on a staggered grid, involving upwinding for the convection terms, and based on Gauss-Seidel and multigrid iteration to solve the resulting nonlinear equations. It was demonstrated that a gradient technique was successful significantly reducing the

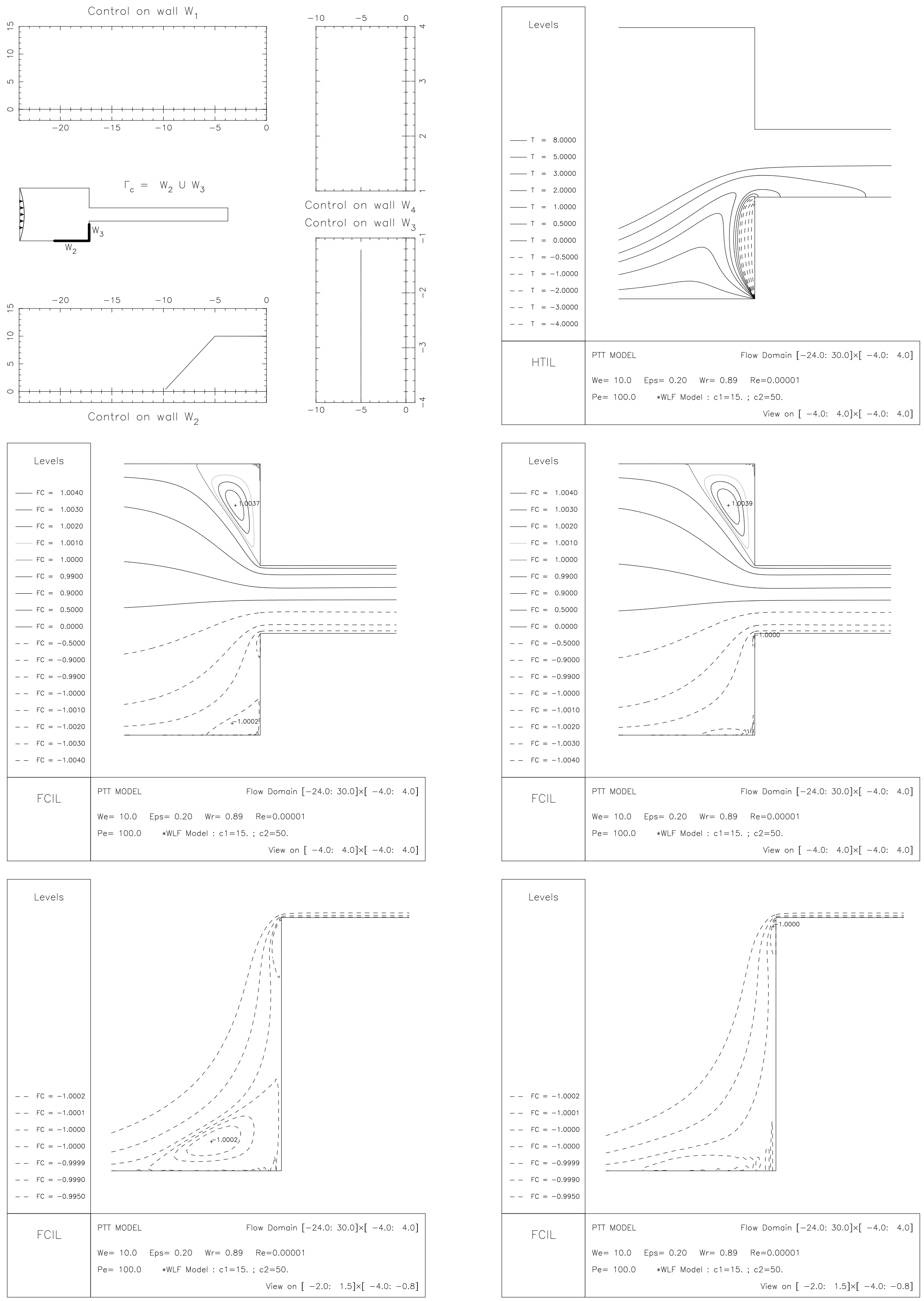

Fig 27: Test 1 : Streamfunction for case -a- (left) and case -b- (right)

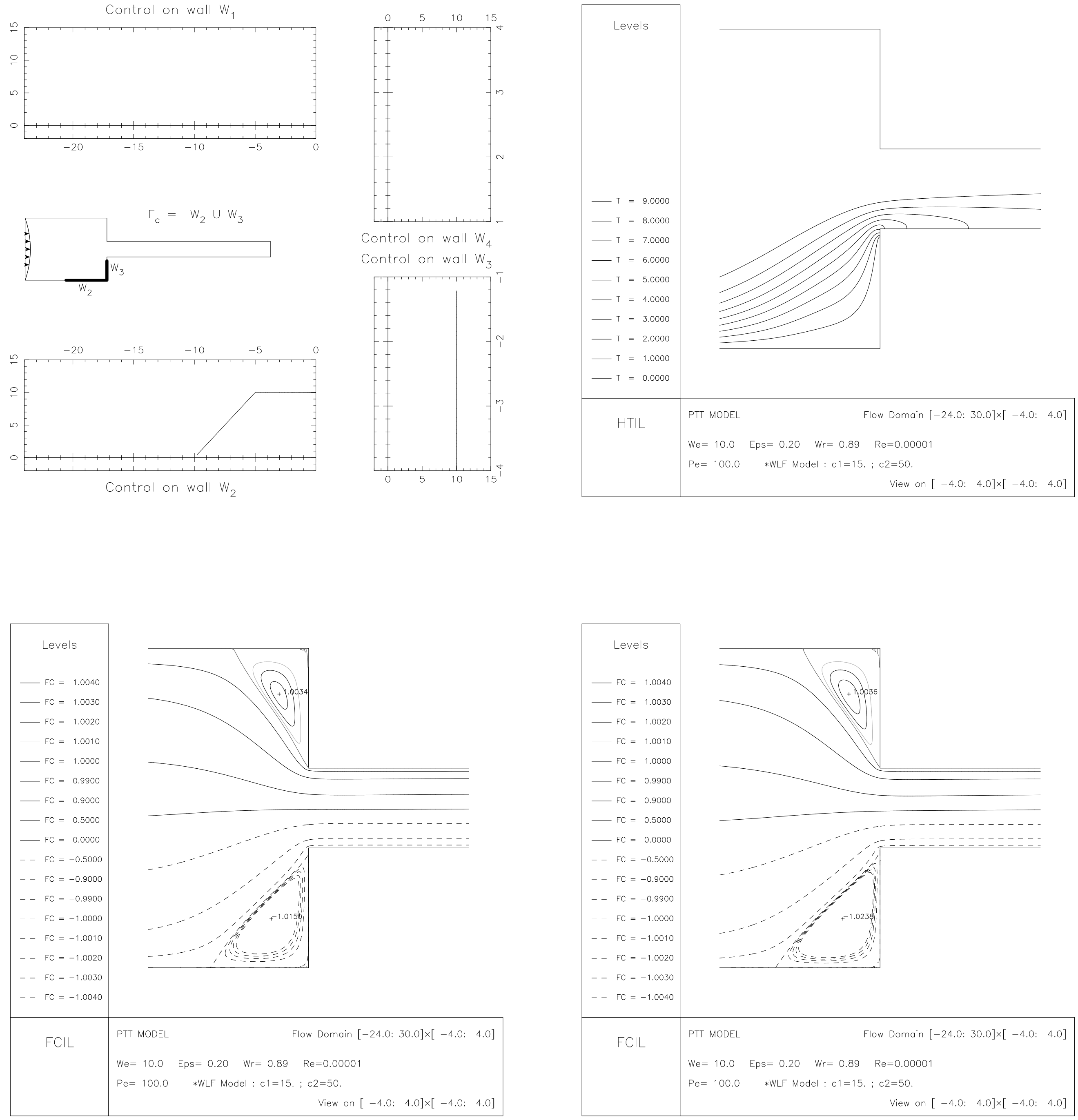

Fig 28: Test 2 : Control (upper left, streamfunction for case -a- (bottom left), heat distribution and streamfunction for case -b- (upper and bottom right)

recirculation region at the entrance from the wide into the narrow part of the channel.

A literature search on previous work on optimal control of viscoelastic flows did not result in any findings.

Many extensions of the present work are possible. Among them are optimal control of evolutionary models for viscoelastic flow, different control mechanisms, and improved optimization techniques to mention just some of them.

A Derivation of the optimality condition

In this section a first order optimality condition for $(\mathcal{P})$ is derived and the expression (4.40) for the gradient of $\mathcal{J}$ is verified. At first several technical lemmas which shall facilitate the computations further below are given.

Throughout U, V and ξ denote two dimensional vector fields defined over the domain Ω with boundary Γ. By $\boldsymbol{\tau}$ and $\boldsymbol{\theta}$ we denote tensor of order two. We utilize the common notation $\nabla U = \begin{pmatrix} \nabla u \\ \nabla v \end{pmatrix}$ where $U = (u, v)$, $\mathbf{D}(\xi) = \frac{1}{2}(\ \nabla\xi + (\nabla\xi)^T\ )$,

$\boldsymbol{\tau} : \boldsymbol{\theta} = \sum_{i,j=1}^{2} \boldsymbol{\tau}_{ij}\boldsymbol{\theta}_{ij}$, Div $\boldsymbol{\tau} = \begin{pmatrix} \partial_x\tau_{11} + \partial_y\tau_{12} \\ \partial_x\tau_{21} + \partial_y\tau_{22} \end{pmatrix}$, and $\partial_i\boldsymbol{\tau} = \begin{pmatrix} \partial_i\tau_{11} & \partial_i\tau_{12} \\ \partial_i\tau_{21} & \partial_i\tau_{22} \end{pmatrix}$.

• **Lemma A.1.** $\displaystyle\int_\Omega (\mathrm{Div}\ \boldsymbol{\tau}) \cdot \xi\ dx = -\int_\Omega \boldsymbol{\tau} : \mathbf{D}(\xi)\ dx + \int_\Gamma \boldsymbol{\tau} : (\xi n^T)\ d\Gamma$,

if $\boldsymbol{\tau}$ is symmetric.

The proofs of this as well as of the following lemmas are rather straightforward and are therefore left to the reader.

• **Lemma A.2.** $\displaystyle\int_\Omega (U\cdot\nabla)\boldsymbol{\tau} : \boldsymbol{\theta}\ dx = -\int_\Omega \boldsymbol{\tau} : (U\cdot\nabla)\boldsymbol{\theta}\ dx + \int_\Gamma (U\cdot n)\boldsymbol{\tau} : \boldsymbol{\theta}\ d\Gamma$,

if div $U = 0$.

• **Lemma A.3.** Let A,B,C denote arbitrary 2×2 matrices. Then we have

(a) $(\mathrm{AB}) : \mathrm{C} = \mathrm{A} : (\mathrm{CB}^T)$,

(b) $(\mathrm{AB}) : \mathrm{C} = \mathrm{B} : (\mathrm{A}^T\mathrm{B})$.

We shall utilize this lemma in the following forms :

$$[\ \boldsymbol{\tau}\ (\nabla U)^T\ ] : \boldsymbol{\theta} = \boldsymbol{\tau} : [\ \boldsymbol{\theta}\ \nabla U\ ] \ , \tag{A.1}$$

$$[\ (\nabla U)\ \boldsymbol{\tau}\ ] : \boldsymbol{\theta} = \boldsymbol{\tau} : [\ \boldsymbol{\theta}\ (\nabla U)^T\ ] \ . \tag{A.2}$$

• **Lemma A.4.** $(U\cdot\nabla)\boldsymbol{\tau} : \boldsymbol{\theta} = U \cdot \begin{pmatrix} \partial_x\boldsymbol{\tau} : \boldsymbol{\theta} \\ \partial_y\boldsymbol{\tau} : \boldsymbol{\theta} \end{pmatrix}$.

• **Lemma A.5.** $\int_\Omega [\boldsymbol{\tau}\ (\nabla U^T)] : \boldsymbol{\theta}\ dx = -\int_\Omega U \cdot [\mathrm{Div}\ (\boldsymbol{\theta}^T \boldsymbol{\tau})]\ dx\ + \int_\Gamma (U n^T) : (\boldsymbol{\theta}^T \boldsymbol{\tau})\ d\Gamma$.

• **Lemma A.6.** $\int_\Omega (\nabla U\ \boldsymbol{\tau}) : \boldsymbol{\theta}\ dx = -\int_\Omega U \cdot [\mathrm{Div}\ (\boldsymbol{\theta}\ \boldsymbol{\tau}^T)]\ dx\ + \int_\Gamma (U n^T) : (\boldsymbol{\theta}\ \boldsymbol{\tau}^T)\ d\Gamma$.

• **Lemma A.7.** $[(V \cdot \nabla) U] \cdot \xi\ = V \cdot [\ (\nabla U^T)\ \xi)\ ]$.

• **Lemma A.8.** $\int_\Omega [(U \cdot \nabla) V] \cdot \xi\ dx = -\int_\Omega V \cdot [(U \cdot \nabla)\xi]\ dx\ + \int_\Gamma V \cdot (U \cdot n)\xi\ d\Gamma$.

The optimality system is derived by means of a Lagrangian technique. For this purpose adjoint variables $(\xi, \pi, \boldsymbol{\theta}, \rho, \mu)$ are introduced and referred to as adjoint velocity, pressure, stress, temperature and control respectively. Further λ_i denote Lagrange multipliers corresponding to the boundary conditions. The Lagrangian is defined by:

$$L(U, p, \boldsymbol{\tau}, T, \mathbf{g}, \mu, \xi, \pi, \boldsymbol{\theta}, \rho, \lambda_i)\ =\ \mathcal{J}(U, \mathbf{g})\ +$$

$$\int_\Omega [\ \mathrm{Re}\ (U \cdot \nabla) U\ - (1-\omega_r)\Delta U + \nabla p - \mathrm{Div}\ \boldsymbol{\tau}\ ] \cdot \xi\ dx\ +\ \int_\Omega (\mathrm{div}\ U)\ \pi\ dx\ +$$

$$\int_\Omega [\ (U \cdot \nabla)\boldsymbol{\tau} - \boldsymbol{\tau} \cdot \nabla U^T - \nabla U \cdot \boldsymbol{\tau} + \frac{1}{\mathrm{We}(T)}(1 + \epsilon \frac{\mathrm{We}}{\omega_r} \mathrm{Tr}(\boldsymbol{\tau}))\boldsymbol{\tau} - 2\frac{\omega_r}{\mathrm{We}}\mathbf{D}\ ] : \boldsymbol{\theta}\ \ dx\ +$$

$$\int_\Omega [(U \cdot \nabla) T - \frac{1}{\mathrm{Pe}}\Delta T\ ]\ \rho\ dx\ \ +\ \int_{\Gamma_c} (T - \mathbf{g})\ \mu\ d\Gamma_c\ +\ \int_{\Gamma_{in}} T\ \lambda_1\ d\Gamma_{in}\ +$$

$$\int_{\Gamma_n} (\frac{\partial T}{\partial n}\ \lambda_2)\ d\Gamma_n\ +\ \int_{\Gamma_{in}} (\boldsymbol{\tau} - \boldsymbol{\tau}_{in})\ \lambda_3\ d\Gamma_{in}\ +\ \int_\Gamma (U - U_b)\ \lambda_4\ d\Gamma \quad ,$$

where $U_b = U_{in}$ on Γ_{in}, $U_b = U_{out}$ on Γ_{out} and $U_b = 0$ elsewhere on Γ.

Note that in the Lagrangian, we have rewritten the equation on $\boldsymbol{\tau}$ by dividing all the terms by $\mathrm{We}(T)$, and that the right-hand-side is no more function of temperature since $\omega_r(T)$ and $\mathrm{We}(T)$ have the same temperature dependence :

$$[\ (U \cdot \nabla)\boldsymbol{\tau} - \boldsymbol{\tau} \cdot \nabla U^T - \nabla U \cdot \boldsymbol{\tau}\ ] + \frac{1}{\mathrm{We}(T)}[1 + \epsilon \frac{\mathrm{We}}{\omega_r}\mathrm{Tr}(\boldsymbol{\tau})]\boldsymbol{\tau} = 2\frac{\omega_r(T)}{\mathrm{We}(T)}\mathbf{D}\ = 2\frac{\omega_r}{\mathrm{We}}\mathbf{D}\ .$$

For all $(\delta U, \delta p, \delta\boldsymbol{\tau}, \delta T, \delta\mathbf{g})$, we must have :

$$L_U(\delta U) + L_p(\delta p) + L_{\boldsymbol{\tau}}(\delta\boldsymbol{\tau}) + L_T(\delta T) + L_{\mathbf{g}}(\delta\mathbf{g}) = 0 \quad . \tag{A.3}$$

This implies, in particular, that

$$
\begin{aligned}
L_p(\delta p) &= + \int_\Omega \nabla(\delta p) \cdot \xi \; dx \\
&= - \int_\Omega \delta p \cdot \mathrm{div}\; \xi \; dx \quad + \int_\Gamma \delta p \; (\xi \cdot n) \; d\Gamma \quad = \; 0 \quad .
\end{aligned}
$$

Choosing δp with support compact in Ω, we obtain

$$
\mathrm{div}\; \xi = 0 \qquad \text{in } \Omega \quad .
$$

Further we find

$$
\begin{aligned}
L_U(\delta U) \;\; = \;\; & + \int_\Omega \mathcal{J}_U \cdot \delta U \; dx \\
& + \int_\Omega [\; \mathrm{Re}(U \cdot \nabla)\delta U \; + \; (\delta U \cdot \nabla)U) \; - (1 - \omega_r)\Delta \delta U \;] \cdot \xi \; dx \\
& + \int_\Omega \mathrm{div}\; (\delta U) \; \pi \; dx \\
& + \int_\Omega [\; (\delta U \cdot \nabla)\boldsymbol{\tau} - \boldsymbol{\tau} \cdot \nabla \delta U^T - \nabla \delta U \cdot \boldsymbol{\tau} \; - 2\frac{\omega_r}{\mathrm{We}}\mathbf{D}(\delta U)] : \boldsymbol{\theta} \; dx \\
& + \int_\Omega (\delta U \cdot \nabla)T \; \rho \; dx \quad + \int_\Gamma \delta U \cdot \lambda_4 \; d\Gamma \quad .
\end{aligned}
$$

Integration by parts and (A.3) lead to

$$
\begin{aligned}
L_U(\delta U) = \;\; & + \int_\Omega \mathcal{J}_U \cdot \delta U \; dx \\
& - \mathrm{Re} \int_\Omega \delta U \cdot (U \cdot \nabla)\xi \; dx \quad + \mathrm{Re} \int_\Gamma \delta U \cdot \xi (U \cdot n) \; d\Gamma \\
& + \mathrm{Re} \int_\Omega \delta U \cdot (\nabla U^T \cdot \xi) \; dx \\
& - \int_\Omega (1 - \omega_r) \delta U \cdot \Delta \xi \; dx - \int_\Gamma (1 - \omega_r) \; [\; \partial_n \delta U \cdot \xi \quad - \quad \delta U \cdot \partial_n \xi \;] \; d\Gamma \\
& - \int_\Omega \delta U \cdot \nabla \pi \; dx \; + \int_\Gamma (\delta U \cdot n) \; \pi \; d\Gamma \\
& + \int_\Omega \delta U \cdot [(\begin{array}{c} \partial_x \boldsymbol{\tau} : \boldsymbol{\theta} \\ \partial_y \boldsymbol{\tau} : \boldsymbol{\theta} \end{array})] \; dx \\
& + \int_\Omega \delta U \cdot \mathrm{Div}\; (\boldsymbol{\theta}^T \boldsymbol{\tau}) \; dx \; - \int_\Gamma (\delta U \; n^T) : (\boldsymbol{\theta}^T \boldsymbol{\tau}) \; d\Gamma \\
& + \int_\Omega \delta U \cdot \mathrm{Div}\; (\boldsymbol{\theta} \boldsymbol{\tau}^T) \; dx \; - \int_\Gamma (\delta U \; n^T) : (\boldsymbol{\theta} \boldsymbol{\tau}^T) \; d\Gamma \\
& + \int_\Omega 2\frac{\omega_r}{\mathrm{We}} (\delta U) \cdot \mathrm{Div}\; \boldsymbol{\theta} \; dx \; - \int_\Gamma 2\frac{\omega_r}{\mathrm{We}} \boldsymbol{\theta} : (\delta U n^T) \; d\Gamma \\
& + \int_\Omega \delta U \cdot (\rho \; \nabla T) \; dx \; + \int_\Gamma \delta U \cdot \lambda_4 \; d\Gamma \quad = \; 0 \quad .
\end{aligned}
$$

Choosing δU with compact support in Ω, all boundary terms vanish and the last equality implies that

$$-\mathrm{Re}\ (U\cdot\nabla)\xi \ + \ \mathrm{Re}\ \nabla U^T\cdot\xi \ - \ (1-\omega_r)\Delta\xi \ - \ \nabla\pi \ + \ \mathcal{J}_U \ + \ \begin{pmatrix} \partial_x\boldsymbol{\tau}:\boldsymbol{\theta} \\ \partial_y\boldsymbol{\tau}:\boldsymbol{\theta} \end{pmatrix}$$

$$+ \ \mathrm{Div}\ (\boldsymbol{\theta}^T\boldsymbol{\tau}) \ + \ \mathrm{Div}\ (\boldsymbol{\theta}\boldsymbol{\tau}^T) \ + \ 2\frac{\omega_r}{\mathrm{We}}\mathrm{Div}\ \boldsymbol{\theta} \ + \ \rho\nabla T \ = \ 0 \quad .$$

So far we derived the first two equations of (D). Next boundary conditions on ξ are obtained restricting δU such that $\delta U = 0$ on $\partial\Gamma$:

$$-\int_\Gamma (1-\omega_r)\ [\ \partial_n\delta U\cdot\xi\ ]\ d\Gamma \ = \ 0 \quad ,$$

so that $\xi = 0$ on Γ follows.

Taking variations with respect to $\delta\boldsymbol{\tau}$ we obtain :

$$\begin{aligned} L_{\boldsymbol{\tau}}(\delta\boldsymbol{\tau}) = \ &+ \int_\Omega -\mathrm{Div}\ (\delta\boldsymbol{\tau})\cdot\xi\ dx \\ &+ \int_\Omega [\ (U\cdot\nabla)\delta\boldsymbol{\tau} - \delta\boldsymbol{\tau}\cdot\nabla U^T - \nabla U\cdot\delta\boldsymbol{\tau}] : \boldsymbol{\theta}\ dx \\ &+ \int_\Omega [\ \frac{\delta\boldsymbol{\tau}}{\mathrm{We}(T)} + \frac{1}{\mathrm{We}(T)}\epsilon\frac{\mathrm{We}}{\omega_r}(\mathrm{Tr}(\delta\boldsymbol{\tau})\boldsymbol{\tau} + \mathrm{Tr}(\boldsymbol{\tau})\delta\boldsymbol{\tau})] : \boldsymbol{\theta}\ dx \\ &+ \int_{\Gamma_{in}} \delta\boldsymbol{\tau} : \lambda_3\ d\Gamma_{in} \quad = \ 0 \quad . \end{aligned}$$

With the rules of calculus and integration by parts we calculate

$$\begin{aligned} L_{\boldsymbol{\tau}}(\delta\boldsymbol{\tau}) \ = \ & \int_\Omega \delta\boldsymbol{\tau} : \mathbf{D}(\xi)\ dx \ - \ \int_\Gamma \delta\boldsymbol{\tau} : (\xi n^T)\ d\Gamma \\ - \ & \int_\Omega \delta\boldsymbol{\tau} : (U\cdot\nabla)\boldsymbol{\theta}\ dx \ + \ \int_\Gamma \delta\boldsymbol{\tau} : (U\cdot n)\boldsymbol{\theta}\ d\Gamma \ - \ \int_\Omega \delta\boldsymbol{\tau} : (\boldsymbol{\theta}\cdot\nabla U + \nabla U^T\cdot\boldsymbol{\theta})\ dx \\ + \ & \int_\Omega \delta\boldsymbol{\tau} : \frac{\boldsymbol{\theta}}{\mathrm{We}(T)}\ dx \ + \ \epsilon\frac{\mathrm{We}}{\omega_r}\int_\Omega \delta\boldsymbol{\tau} : \frac{1}{\mathrm{We}(T)}[\mathrm{Tr}(\boldsymbol{\tau})\boldsymbol{\theta} + (\boldsymbol{\tau}:\boldsymbol{\theta})\mathbf{I}]\ dx \\ + \ & \int_{\Gamma_{in}} \delta\boldsymbol{\tau} : \lambda_3\ d\Gamma_{in} \quad = \ 0 \quad . \end{aligned}$$

The equation for $\boldsymbol{\theta}$ now directly follows :

$$\mathrm{We}(T)[\ -(U\cdot\nabla)\boldsymbol{\theta} \ - \ \boldsymbol{\theta}\cdot\nabla U \ - \ \nabla U^T\cdot\boldsymbol{\theta}\ ] + \boldsymbol{\theta} \ + \ \epsilon\frac{\mathrm{We}}{\omega_r}[\mathrm{Tr}(\boldsymbol{\tau})\boldsymbol{\theta} + (\boldsymbol{\tau}:\boldsymbol{\theta})\mathbf{I}] = -\ \mathrm{We}(T).\mathbf{D}(\xi)\ .$$

<u>Boundary conditions on $\boldsymbol{\theta}$:</u> As for the boundary conditions for $\boldsymbol{\theta}$ we utilize the fact that $\xi = 0$ on Γ so that

$$\lambda_3{\cdot}\chi_{\Gamma_{in}} \ + \ (U\cdot n)\ \boldsymbol{\theta} \ = 0 \quad \text{on } \Gamma \quad .$$

This implies that $\boldsymbol{\theta} = 0$ on Γ_{out} since $U \cdot n \neq 0$ there. Since $U \cdot n = 0$ on $\Gamma \setminus (\Gamma_{in} \cup \Gamma_{out})$, there is no boundary condition for $\boldsymbol{\theta}$ on $\Gamma \setminus (\Gamma_{in} \cup \Gamma_{out})$. On Γ_{in} as well $\boldsymbol{\theta}$ does not satisfy boundary condition and $\lambda_3 = -(U \cdot n)\ \boldsymbol{\theta}$ on Γ_{in} .

Taking variations with respect to δT we find

$$\begin{aligned} L_T(\delta T) \ = \ + & \int_\Omega [\ (U \cdot \nabla)\delta T \ - \ \frac{1}{\mathrm{Pe}} \Delta \delta T]\ \rho\ dx \\ + & \int_\Omega (\frac{1}{\mathrm{We}})'(T)[\delta T(\boldsymbol{\tau} + \epsilon \frac{\mathrm{We}}{\omega_r} \mathrm{Tr}(\boldsymbol{\tau})\boldsymbol{\tau})\ ] : \boldsymbol{\theta}\ dx \\ + & \int_{\Gamma_c} \delta T\ \mu\ d\Gamma_c \ + \ \int_{\Gamma_{in}} \delta T\ \lambda_1\ d\Gamma_{in} \ + \ \int_{\Gamma_n} \partial_n(\delta T)\ \lambda_2\ d\Gamma_n \ = \ 0 \ , \end{aligned}$$

and further

$$\begin{aligned} L_T(\delta T) \ = \ - & \int_\Omega \delta T\ (U \cdot \nabla)\rho\ dx \ + \int_\Gamma \delta T\ (U \cdot n)\ \rho\ d\Gamma \\ - & \int_\Omega \delta T\ \frac{1}{\mathrm{Pe}} \Delta\rho\ dx \ - \frac{1}{\mathrm{Pe}} \int_\Gamma [\ \partial_n(\delta T)\ \rho \ - \ \delta T\ \partial_n \rho\ ]\ d\Gamma \\ + & \int_\Omega \delta T\ (\frac{1}{\mathrm{We}})'(T)[1 + \epsilon \frac{\mathrm{We}}{\omega_r} \mathrm{Tr}(\boldsymbol{\tau})]\boldsymbol{\tau} : \boldsymbol{\theta}\ \ dx \\ + & \int_{\Gamma_c} \delta T\ \mu\ d\Gamma_c \ + \int_{\Gamma_{in}} \delta T\ \lambda_1\ d\Gamma_{in} \ + \int_{\Gamma_n} \partial_n(\delta T).\lambda_2\ d\Gamma_n \ \ = \ 0 \ , \end{aligned}$$

which implies, for δT with compact support in Ω :

$$- \ (U \cdot \nabla)\rho \ - \ \frac{1}{\mathrm{Pe}} \Delta\rho \ + \ (\frac{1}{\mathrm{We}})'(T)[1 + \epsilon \frac{\mathrm{We}}{\omega_r} \mathrm{Tr}(\boldsymbol{\tau})]\boldsymbol{\tau} : \boldsymbol{\theta} \ = 0 \ \ ,$$

so that the first four equations in (D) are satisfied.

<u>Boundary conditions on ρ :</u> when choosing δT such that $\partial_n \delta T \ = 0$, we obtain

$$(U \cdot n)\rho \ + \ \frac{1}{\mathrm{Pe}}\ \partial_n \rho \ + \ \mu.\chi_c \ + \ \lambda_1.\chi_{in} \ = 0 \ \ . \tag{A.4}$$

Considering $\Gamma_n = \Gamma \setminus (\Gamma_c \cup \Gamma_{in})$, we have :
 if $U \cdot n = 0$ then $\partial_n \rho = 0$ (i.e. on fixed walls minus Γ_c),
 if $U \cdot n \neq 0$ then $\frac{1}{\mathrm{Pe}} \partial_n \rho + u\rho = 0$ (i.e. on Γ_{out}).

When choosing δT such that $\delta T = 0$ on Γ, we obtain $-\frac{1}{\mathrm{Pe}}\ \rho \ + \lambda_2\ \chi_{\Gamma_n} \ = \ 0$, so that outside Γ_n we have $\rho = 0$.

Finally taking variations with respect to $\delta \mathbf{g}$ we find that $\mu = \gamma.\mathbf{g}$ on Γ_c which by (A.4) implies that

$$\gamma.\mathbf{g} = -\frac{1}{\mathrm{Pe}}\ \partial_n \rho \quad \text{on } \Gamma_c \tag{OC}$$

This concludes our verification that (P) (BC) (D) and (OC) constitute a first order optimality system for $(\mathcal{P})$.

Finally we need to argue that (4.40) provides an expression for the gradient of the mapping $\mathbf{g} \to \mathcal{J}(\mathbf{g})$. For this purpose we express $(\mathcal{P})$ as

$$\begin{cases} \min \ \boldsymbol{J}(y, \mathbf{g}) \\ e(y, \mathbf{g}) = 0 \end{cases} ,$$

where y represents the state variables $(U, p, \boldsymbol{\tau}, T)$, $e(y, \mathbf{g})$ represents all equality constraints in (P) and $\boldsymbol{J}$ has the same action as $\mathcal{J}$ in $(\mathcal{P})$ but with y and $\mathbf{g}$ treated as independent variables. (In fact, in our case the dependence of $\boldsymbol{J}$ on y reduces to dependence on U). Taking the directional derivatives of $\mathcal{J}$ at $\mathbf{g}$ in direction $\delta\mathbf{g}$ results in

$$(\nabla \mathcal{J}(\mathbf{g}), \delta\mathbf{g}) \ = \ (\nabla_y \boldsymbol{J}(y, \mathbf{g}), \delta y) \ + \ (\nabla_{\mathbf{g}} \boldsymbol{J}(y, \mathbf{g}), \delta\mathbf{g}) \tag{A.5}$$

where δy satisfies

$$(e_y(y, \mathbf{g}), \delta y) \ + \ (e_{\mathbf{g}}(y, \mathbf{g}), \delta\mathbf{g}) \ = \ 0 \ .$$

Assuming that e_y is invertible (which is equivalent to assuming that the linearised equations in (P) have a solution for arbitrary right hand sides), we find

$$\delta y = -e_y(y, \mathbf{g})^{-1} e_{\mathbf{g}}(y, \mathbf{g}) \delta\mathbf{g} \ .$$

Inserting this equation in (A.5) we obtain

$$\begin{aligned} (\nabla \mathcal{J}(\mathbf{g}), \delta\mathbf{g}) \ &= \ (\nabla_y \boldsymbol{J}(y, \mathbf{g}), -e_y(y, \mathbf{g})^{-1} e_{\mathbf{g}}(y, \mathbf{g}) \delta\mathbf{g}) + \ (\nabla_{\mathbf{g}} \boldsymbol{J}(y, \mathbf{g}), \delta\mathbf{g}) \\ &= \ (\lambda, e_{\mathbf{g}}(y, \mathbf{g}) \delta\mathbf{g}) + \ (\nabla_{\mathbf{g}} \boldsymbol{J}(y, \mathbf{g}), \delta\mathbf{g}) \ . \end{aligned}$$

where the 'adjoint' variable λ is the solution to the linearised adjoint equation

$$e_y^{\star} \lambda = -\nabla_y \boldsymbol{J}(y, \mathbf{g}) \ . \tag{A.6}$$

It follows that the gradient of $\mathcal{J}$ is given by

$$\nabla \mathcal{J} = e_{\mathbf{g}}^{\star} \lambda + \nabla_{\mathbf{g}} \boldsymbol{J}(y, \mathbf{g}) \tag{A.7}$$

Applying (A.7) to $(\mathcal{P})$ implies (4.40).

References

[1] F. Abergel, R. Temam. "On Some Control Problems in Fluid Mechanics". Theoret. Comput. Fluid Dynamics(1990) 1:303-325.

[2] R.B. Bird, O. Hassager, R.C. Armstrong and C.F. Curtiss. "Dynamics of Polymeric Liquids". John Wiley and Sons.

[3] A. Brandt. "Multi-level adaptative solutions to boundary value problems". Math. of Comput. 31 333-390(1977).

[4] H. Braun. "A model for the Thermo-rheological Behaviour of Viscoelastic Fluids". Rheol Acta 30:523-529(1991).

[5] H. Choi, R. Temam, P. Moin and J.Kim. "Feedback control for unsteady flow and its application to the stochastic Burger equation". J. Fluid Mech. 253 (1993) 509-543.

[6] M.A. McClelland and B.A. Finlayson. "Heat Transfer effects in extrudate swell of elastic liquids". Journal of Non-Newtonian Fluid Mechanics, 27(1988) 363-374.

[7] A.V. Fursikov, M.D. Gunzburger and L.S. Hou. "Boundary value problems and optimal boundary control for the Navier-Stokes system : the two dimensional case". To appear in SIAM Journal on Control and Optimization.

[8] M. Gad-el-Hak, A. Pollard, J.P. Bonnet. "Flow Control. Fundamentals and Practices". Springer, 1998

[9] R. Glowinsky. "Finite element methods for the numerical simulation of incompressible viscous flows. Introduction to the control of the Navier-Stokes equations." Lectures in Applied Mathematics, Volume 28, pp.219-301 (1991).

[10] M.D. Gunzburger, L.S. Hou, T.P. Svobony. "The approximation of boundary control problems for fluids flows with application to control by heating and cooling". Computers Fluids Vol 22, No 2/3 pp.239-251, 1993.

[11] M.D. Gunzburger "Flow control". Springer, 1995

[12] R.K. Gupta and A.B.Metzner. "Modelling of Non-Isothermal Polymer Process". Journal of Rheology, 26(1982) 181-198.

[13] K. Ito and S.S. Ravindran. "Optimal control of thermally convected fluid flows". SIAM J. Scientific Computing 19, No 6, pp.1870-1891(1998).

[14] K. Ito and S.S. Ravindran. "Reduced order basis for optimal control of unsteady viscous flows" Submitted to Journal of Guidance, Control and Dynamics.

[15] C. Jouron, C.H. Bruneau. "An efficient scheme for solving steady incompressible Navier-Stokes equations". Journal Comput Phys. 89,2, 389-413, 1990.

[16] K. Kunisch and M. Hinze. "Suboptimal control strategies for backwards facing step flows". Proceedings of 15th IMACS World Congress on Scientific Computation, Modelling and Applied Mathematics, Editor A. Sydow, Vol. 3, 53-58, 1997.

[17] Y.S. Ko and A.S. Lodge. "Viscous Heating correction for thermally developing flows in slit die viscometry". Rheol Acta 30:357-368(1991).

[18] X.L. Luo and R.I Tanner. "A pseudo-time integral method for non-isothermal viscoelastic flows and its application to extrusion simulation". Rheology Acta 26:499-507 (1987)

[19] X. Marduel. These de doctorat de l'Université Paris-Sud Orsay. "Simulations Numeriques d'écoulements de fluides viscoelastiques".

[20] H. Al.Moatassime. These de doctorat de l'Université Paris-Sud Orsay. "Simulations Numeriques d'écoulements permanents de fluides non-newtoniens par une methode multigrille".

[21] J.G. Oldroyd. "On the formation of rheological equation of state". Proc. Roy. Soc. A200, 523-541 (1950).

[22] G.W.M. Peters and F.T.P. Baaijens. "Modelling of non-isothermal viscoelastic flows" Journal of Non-Newtonian Fluid Mechanics, 68 (1997) 205-224.

[23] N. Phan-Thien. "A Non Linear Network Viscoelastic Model". Journal of Rheology, 23 (1979) 451.

[24] R.Srinivasan and B.A.Finlayson. "Corrections for the Non-Isothermal Hole Pressure Problem". Journal of Non-Newtonian Fluid Mechanics, 27 (1988) 1-15.

[25] F. Sugend, N. Phan-Thien and R.I. Tanner. "A study of Non-Isothermal Non-Newtonian Extrudate Swell by a Mixed Boundary Element and Finite Element Method". Journal of Rheology 31(1), 37-58 (1987).

[26] R.I. Tanner. "Engineering Rheology". Oxford University Press, London, 1985

[27] C.L. Tucker. "Fundamentals of computer modelling for polymer processing". Hanser Publishers, 1989.

[28] R.K. Upadhya and A.I. Isayev. "Non-Isothermal Elongational Flow of Polymeric Fluids According to the Leonov Model". Journal of Rheology, 28(5), 581-599(1984).

[29] K. Visscher and P.F. Mijnlieff. "Temperature and Concentration dependent viscosity and gelation temperature of ABA triblock copolymer solutions". Rheol Acta 30:559-574(1991).

[30] J.M. Wiest and N. Phan-Thien. "Non-Isothermal Flow of Polymer Melts". Journal of Non-Newtonian Fluid Mechanics, 27 (1989) 333-347.